

Chapter 4

The Limit Cycles Induced by The Disturbance Observer

4.1 Introduction:

In recent years, disturbance observer is generally introduced into motion control systems, to eliminate the unwanted disturbance and plant uncertainty. The disturbance observer has a drawback in regulating control, however. While the system is reaching the desired position, the mutual effect between the disturbance observer and the quantization coming from the sensor and digital to analog converter will induce limit cycles, which will cause large steady-state error in point-to-point control [90]. Therefore, the applicability of the disturbance observer for the regulating control becomes questionable. M. Fischer and M. Tomizuka [95] chose suitable controller parameters from several experimental results to reduce the effect of the limit cycles. But simultaneously, it is difficult to maintain the best transient performance. In this chapter, for the absence of zero-input limit cycles in nonlinear discrete time systems, we will use the theorem [91] to derive sufficient conditions that can avoid limit cycles induced by disturbance observer and quantization. This sufficient condition will help us find adequate controller parameters in velocity loop to avoid the unwanted limit cycles. After that, we will introduce an adaptive parameters mechanism which not only maintains the tracking performance in transient

but also eliminates the limit cycle in steady state. The remainder sections of this chapter are listed as below: In Section 4.2, the sufficient condition for the absence of limit cycle caused by mutual effect between disturbance observer and quantization. Application in the motion control systems and an adaptive parameters mechanism are introduced in Section 4.3 and Section 4.4 respectively. The experimental results are shown in Section 4.5. And finally, the summary of this chapter is discussed in Section 4.6.

4.2 The sufficient condition for the absence of limit cycle caused by mutual effect between disturbance observer and quantization:

The most widespread controller structure adopted in motion control systems is illustrated in figure 4.1.

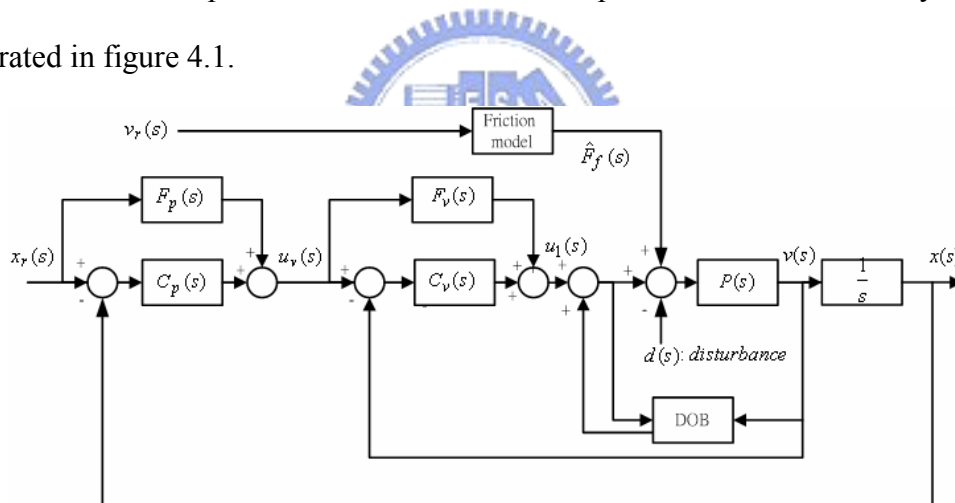


Figure 4.1 Controller structure of the experiment

The controller type of $C_p(s)$ and $C_v(s)$ in position loop and velocity loop can be any common used controller except for integrator in position loop, which will induce severe limit cycles caused by friction [92]. Therefore, the position loop controller which we recommend here is P control. The velocity loop controller is PI control. The feed-forward controller $F_p(s)$ in position loop is a pure differentiator and $F_v(s)$ in velocity loop is the inverse of the plant $P(s)$. The friction compensator based on

the LueGre model is feed-forward type. The moment to generate limit cycle can be described as follow: We give a position command illustrated in figure 4.2. (The profile of figure 4.3 is the velocity command relative to this position command.) When the system reaches the desired position after acceleration-deceleration mechanism within 0~0.25(sec), the signal $u_v(s)$ (see figure 4.1) fed into the velocity loop is almost zero because the signal (velocity command) comes from feed-forward controller $F_p(s)$ is zero and the signal from $C_p(s)$ is extremely small. At this moment , the signal to noise ratio (SNR) in the velocity loop is too low, that the precision of the system is seriously affected by the quantization error coming from encoder and digital to analog converter (DAC). Therefore, the velocity loop which has disturbance observer inside is sustained to correct the errors and generates anxiety limit cycles.

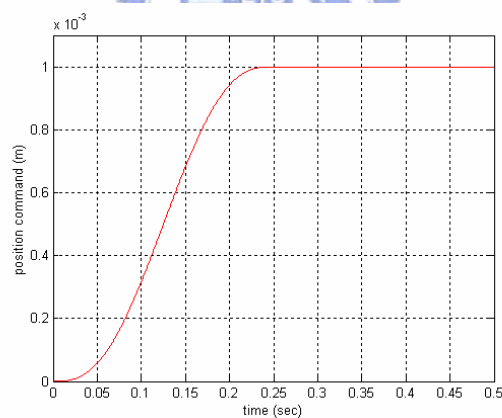


Figure 4.2 The typical position command in regulating control.

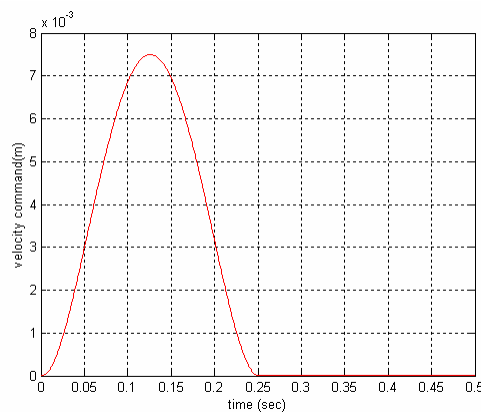


Figure 4.3 The velocity command relative to position command in figure 4.2.

Therefore, we will focus our attention to the velocity loop that has disturbance observer in the inner loop (see figure 4.4) and utilize the theorem [91] for the absence of zero-input limit cycles in nonlinear discrete time systems to derive sufficient conditions that can avoid limit cycle induced by disturbance observer and quantization.

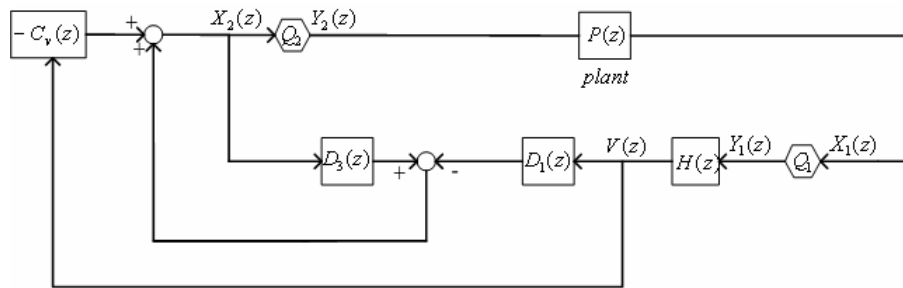


Figure 4.4 Velocity loop of the controller structure in the figure 4.1

We have two assumptions in our analysis:

(a). The friction can be compensated completely by feed-forward type compensator based on LueGre model or disturbance observer, so we can omit the effect of the friction.

(b). The limit cycle caused by the mutual effect between the disturbance observer and quantization only has harmonic components with no DC component, i.e., a pure periodic unbiased signal. This assumption makes sense when we go to the experimental results in section 5.

$H(z)$ in figure 4.4 is the discrete transfer function from sensor output to velocity $V(z)$. If the sensor were a tachometer, $H(z)$ would have a constant. If the sensor were a encoder, $H(z)$ would not have a constant. Q_1 is the truncation type quantizer which comes from sensor. Q_2 is the truncation type quantizer which comes from DAC. The quantizers Q_1 and Q_2 conform to both of the two conditions listed as below:

$$Q(0) = 0 \quad (4.1)$$

$$0 \leq \frac{Q(x)}{x} \leq 1, \quad \forall x \neq 0 \quad (4.2)$$

If the system has a limit cycle of which period length is N samples, we will define a function Λ .

$$\Lambda = N \cdot \sum_{k=0}^{N-1} \{Q_1[x_1(k)] \cdot (x_1(k) - Q_1[x_1(k)]) + Q_2[x_2(k)] \cdot (x_2(k) - Q_2[x_2(k)])\} \quad (4.3)$$

$x_1(k)$: signal before sensor quantizer Q_1 in time domain

$x_2(k)$: signal before DAC quantizer Q_2 in time domain

According to conditions (4.1) and (4.2), the function Λ is always positive and can be rewritten as below:

$$\Lambda = N \cdot \sum_{k=0}^{N-1} \{y_1(k) \cdot (x_1(k) - y_1(k)) + y_2(k) \cdot (x_2(k) - y_2(k))\} \geq 0 \quad (4.4)$$

$y_1(k)$: signal after sensor quantizer Q_1 in time domain

$y_2(k)$: signal after DAC quantizer Q_2 in time domain

Then, we utilize discrete Parseval's theorem to transfer the function Λ into frequency domain representation.

$$\begin{aligned} \Lambda &= \sum_{l=0}^{N-1} \{Y_1^*(z_l) \cdot (X_1(z_l) - Y_1(z_l)) + Y_2^*(z_l) \cdot (X_2(z_l) - Y_2(z_l))\} \geq 0 \\ &= \sum_{l=0}^{N-1} \{Y_1^*(z_l) \cdot (P(z_l) \cdot Y_2(z_l) - Y_1(z_l)) + Y_2^*(z_l) \cdot (B(z_l) \cdot Y_1(z_l) - Y_2(z_l))\} \geq 0 \end{aligned} \quad (4.5)$$

where $z_l = e^{j(2\pi/N)l}$, $B(z_l)$ is the discrete transfer function from $Y_1(z_l)$ to

$X_2(z_l)$. Equation (4.5) can be written by the matrix form.

$$\Lambda = \sum_{l=0}^{N-1} [Y_1^*(z_l) \quad Y_2^*(z_l)] \cdot \begin{bmatrix} -1 & P(z_l) \\ B(z_l) & -1 \end{bmatrix} \cdot \begin{bmatrix} Y_1(z_l) \\ Y_2(z_l) \end{bmatrix} \geq 0 \quad (4.6)$$

let $\vec{Y}(z_l) = [Y_1(z_l) \ Y_2(z_l)]^T$, $\vec{Y}^*(z_l)$ is the conjugate complex transpose of $\vec{Y}(z_l)$,

and $A(z_l) = \begin{bmatrix} -1 & P(z_l) \\ B(z_l) & -1 \end{bmatrix}$, equation (4.6) can be rewritten as below:

$$\Lambda = \sum_{l=0}^{N-1} \vec{Y}^*(z_l) \cdot A(z_l) \cdot \vec{Y}(z_l) \quad (4.7)$$

$A_H(z_l) = \frac{1}{2} \cdot (A(z_l) + A^*(z_l))$ is Hermitian part of $A(z_l)$,

$A_{SH}(z_l) = \frac{1}{2} \cdot (A(z_l) - A^*(z_l))$ is skew Hermitian part of $A(z_l)$. Therefore, equation

(4.7) can be written by the form.

$$\Lambda = \sum_{l=0}^{N-1} [\vec{Y}^*(z_l) \cdot A_H(z_l) \cdot \vec{Y}(z_l) + \vec{Y}^*(z_l) \cdot A_{SH}(z_l) \cdot \vec{Y}(z_l)] \quad (4.8)$$

Because the value of $\vec{Y}^*(z_l) \cdot A_H(z_l) \cdot \vec{Y}(z_l)$ is only real, $\vec{Y}^*(z_l) \cdot A_{SH}(z_l) \cdot \vec{Y}(z_l)$ is

zero or pure imaginary, so $\vec{Y}^*(z_l) \cdot A_H(z_l) \cdot \vec{Y}(z_l)$ is the real part of

$\vec{Y}^*(z_l) \cdot A(z_l) \cdot \vec{Y}(z_l)$ and $\vec{Y}^*(z_l) \cdot A_{SH}(z_l) \cdot \vec{Y}(z_l)$ is the imaginary part of

$\vec{Y}^*(z_l) \cdot A(z_l) \cdot \vec{Y}(z_l)$.

$$\vec{Y}^*(z_l) \cdot A_H(z_l) \cdot \vec{Y}(z_l) = \text{Re}(\vec{Y}^*(z_l) \cdot A(z_l) \cdot \vec{Y}(z_l)) \quad (4.9)$$

$$\vec{Y}^*(z_l) \cdot A_{SH}(z_l) \cdot \vec{Y}(z_l) = \text{Im}(\vec{Y}^*(z_l) \cdot A(z_l) \cdot \vec{Y}(z_l)) \quad (4.10)$$

In equation (4.7), the value of $\vec{Y}^*(z_l) \cdot A(z_l) \cdot \vec{Y}(z_l)$ for $l = 1 \sim (\frac{N}{2} - 1)$ and

$l = (\frac{N}{2} + 1) \sim (N - 1)$ are conjugate complex. Therefore, function Λ can be rewritten

by the form.

$$\Lambda = \vec{Y}^*(z_0) \cdot A(z_0) \cdot \vec{Y}(z_0) + 2 \cdot \sum_{l=1}^{\frac{N-1}{2}} \text{Re}(\vec{Y}^*(z_l) \cdot A(z_l) \cdot \vec{Y}(z_l)) + \vec{Y}^*(z_{N/2}) \cdot A(z_{N/2}) \cdot \vec{Y}(z_{N/2})$$

Because the limit cycle is a pure harmonic signal, $\vec{Y}(z_0) = \vec{0}$.

Since $\vec{Y}^*(z_{N/2}) \cdot A(z_{N/2}) \cdot \vec{Y}(z_{N/2})$ only has real part, the above equation can be

rewritten as below.

$$\Lambda = 2 \cdot \sum_{l=1}^{\frac{N-1}{2}} \text{Re}(\bar{Y}^*(z_l) \cdot A(z_l) \cdot \bar{Y}(z_l)) + \text{Re}(\bar{Y}^*(z_{N/2}) \cdot A(z_{N/2}) \cdot \bar{Y}(z_{N/2})) \quad (4.11)$$

Take equation (4.9) into equation (4.11).

$$\Lambda = 2 \cdot \sum_{l=1}^{\frac{N-1}{2}} \bar{Y}^*(z_l) \cdot A_H(z_l) \cdot \bar{Y}(z_l) + \bar{Y}^*(z_{N/2}) \cdot A_H(z_{N/2}) \cdot \bar{Y}(z_{N/2}) \quad (4.12)$$

Given that $A_H(z_l)$ is negative definite ($A_H(z_l) < 0$) for $l = 1 \sim \frac{N}{2}$, then the right-hand side of the equation (4.12) is always negative, but the left-hand side Λ is always positive or zero. Thus, the right-hand side of the equation (4.12) contradicts the fact $\Lambda \geq 0$. The only condition to avoid the contradiction is $\bar{Y}(z_l) = \vec{0}$ for $l = 1 \sim \frac{N}{2}$, and no limit cycles will generate. $A_H(z_l)$ is negative definite is the sufficient condition for the absence of zero-input limit cycles. Therefore, If we could design the controller parameters to make $A_H(z_l)$ is negative definite for $l = 1 \sim \frac{N}{2}$, the system would not have generated limit cycles. Let's get the eigenvalue of $A_H(z_l)$.

$$A_H(z_l) = \begin{bmatrix} -1 & \frac{P(z_l) + B^*(z_l)}{2} \\ \frac{(P(z_l) + B^*(z_l))^*}{2} & -1 \end{bmatrix}$$

$$|\lambda \cdot I - A_H(z_l)| = 0$$

$$\begin{vmatrix} \lambda + 1 & -\frac{(P(z_l) + B^*(z_l))}{2} \\ -\frac{(P(z_l) + B^*(z_l))^*}{2} & \lambda + 1 \end{vmatrix} = 0$$

$$\lambda^2 + 2 \cdot \lambda + 1 - \frac{|P(z_l) + B^*(z_l)|^2}{4} = 0 \quad (4.13)$$

If all coefficients in the polynomial (4.13) are positive, the eigenvalue λ of $A_H(z_l)$

is all negative. Therefore, $A_H(z_l)$ is negative definite Hermitian matrix and satisfies the sufficient condition for the absence of limit cycles.

$$1 - \frac{|P(z_l) + B^*(z_l)|^2}{4} > 0$$

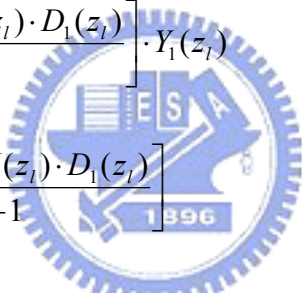
$$\frac{|P(z_l) + B^*(z_l)|^2}{4} < 1$$

$$|P(z_l) + B^*(z_l)| < 2 \quad (4.14)$$

Now, we will get the discrete transfer function $B(z_l)$. Let's take a close look at the path from $Y_1(z_l)$ to $X_2(z_l)$ in figure 4.4.

$$-Y_1(z_l) \cdot H(z_l) \cdot C_v(z_l) + [X_2(z_l) \cdot D_3(z_l) - Y_1(z_l) \cdot H(z_l) \cdot D_1(z_l)] = X_2(z_l)$$

$$X_2(z_l) = \left[\frac{H(z_l) \cdot C_v(z_l) + H(z_l) \cdot D_1(z_l)}{D_3(z_l) - 1} \right] \cdot Y_1(z_l)$$



$$\text{so } B(z_l) = \left[\frac{H(z_l) \cdot C_v(z_l) + H(z_l) \cdot D_1(z_l)}{D_3(z_l) - 1} \right] \quad (4.15)$$

Take (4.15) into (4.14):

$$\left| P(z_l) + \left(\frac{H(z_l) \cdot C_v(z_l) + H(z_l) \cdot D_1(z_l)}{D_3(z_l) - 1} \right)^* \right| < 2 \quad \text{for } l=1 \sim \frac{N}{2} \quad (z_l = e^{j(2\pi/N)l}) \quad (4.16)$$

Finally, the inequality (4.16) which occurs in the velocity loop of the system illustrated in figure 4.4 is the sufficient condition for the absence of zero-input limit cycles caused by the mutual effect between disturbance observer and quantization.

Theorem: The N length limit cycles induced by disturbance observer and quantization are absent from the velocity loop illustrated in figure 4.4, if the following condition is satisfied.

$$\left| P(z_l) + \left(\frac{H(z_l) \cdot C_v(z_l) + H(z_l) \cdot D_1(z_l)}{D_3(z_l) - 1} \right)^* \right| < 2 \quad \text{for } l=1 \sim \frac{N}{2} \quad (z_l = e^{j(2\pi/N) \cdot l})$$

(proof as above paragraph)

4.3 Application in the motion control systems:

To verify the validity of the inequality (4.16), we will give two examples : (1). The motion control structure proposed by H. Kobayashi [90]. (2). The structure (figure 4.1) we used in our systems.

(1).The motion control structure proposed by H. Kobayashi is illustrated in the figure 4.5.

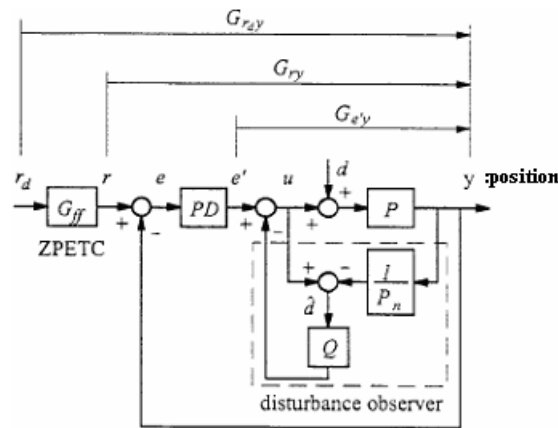


Figure 4.5 The motion control structure proposed by H. Kobayashi (H. Kobayashi 1996[90])

According to figure 4.5 proposed by H. Kobayashi[90] we know that the system only has position loop but doesn't have velocity loop, so the $C_v(z_l)$ in the inequality (4.16) applied in the system is set to zero. The inverse plant transfer function $P^{-1}(s)$ in the system is from position to voltage, not from velocity to voltage. So, the $H(z_l)$ equals 1 and the continuous transfer function $P^{-1}(s)$ designed by H. Kobayashi is listed as below:

$$P^{-1}(s) = \frac{s \cdot (J \cdot s + B)}{k_t \cdot k_a}$$

J :inertia (kg)

B :viscous friction coefficient (kg/sec)

k_a :gain of current driver (A/Volt)

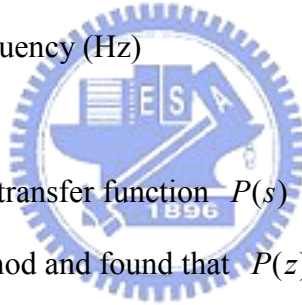
k_t :force constant of motor(Nt/A)

The author used a third order low-pass filter $Q(s)$ to make $P^{-1}(s)$ become realizable.

$$Q(s) = \frac{3 \cdot \tau \cdot s + 1}{(\tau \cdot s + 1)^3}$$

$$\tau = \frac{1}{2 \cdot \pi \cdot B_w}$$

B_w :low-pass filter cut-off frequency (Hz)



He transferred the continuous transfer function $P(s)$ into discrete transfer function $P(z)$ by zero-order hold method and found that $P(z)$ had zero near -1.

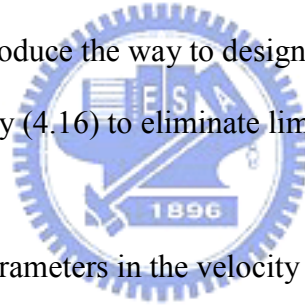
Consequently, $P^{-1}(z)$ in the disturbance observer had pole near -1 (has pole near $\pm j \frac{\omega_s}{2}$ in s domain. ω_s :Sampling frequency(rad/sec)). The author considered the outcome became the reason why the system generated limit cycles. Disregarding the nature of the system, he moved the pole of $P^{-1}(z)$ much more inside the unit circle by a parameter r , see equation (4.17).

$$P^{-1}(z^{-1}) = \frac{1 + a_1 \cdot z^{-1} + a_2 \cdot z^{-2}}{(b_1 + r) \cdot z^{-1} + (b_2 - r) \cdot z^{-2}} \quad (4.17)$$

The author moved the pole of $P^{-1}(z)$ to -0.6, and the experimental results showed that the limit cycles could be reduced but not eliminated.

If we take $P^{-1}(z)$ with pole near -1 into the inequality (4.16), we are not able to find parameters which satisfy the sufficient condition, even if we lower the cut-off

frequency of the low-pass filter in the disturbance observer to a very low value (1hz). Similar to the method introduced by H. Kobayashi, the only solution to satisfy the inequality (4.16) is to move the pole of $P^{-1}(z)$ much more away from -1 pole. The parameters that can satisfy the sufficient condition are the pole of $P^{-1}(z)$ on the right-hand side (approximately on the 0.98 pole), and 1 hz of the low-pass filter cut-off frequency. Therefore, the condition satisfying the inequality (4.16) for the absence of the limit cycle is much more stringent than the condition derived from H. Kobayashi's method, but the ways to reduce limit cycles are roughly the same. Besides, the inverse plant $P^{-1}(z)$ in our system (see figure 4.1) is designed by pole-zero matched method and doesn't have pole on the left-hand side like H. Kobayashi's systems. But our system still generates limit cycles. In the next paragraph, we will briefly introduce the way to design controller parameters of our system which satisfy inequality (4.16) to eliminate limit cycles.



(2). In order to find a set of parameters in the velocity loop which can not generate limit cycles caused by disturbance observer and quantization, we will apply the sufficient conditions to the motion control system introduced in section 2 (see figure 4.1). In this system, the sensor is encoder, so the discrete transfer function $H(z)$ is a $\alpha - \beta$ filter [82] that can differentiate the position measured from the encoder with respect to time to obtain the velocity $V(z)$. The $\alpha - \beta$ filter we used here is critical damping second order type and $H(z)$ is listed as below: (all discrete transfer function in this chapter will be expressed as z^{-1} form)

$$H(z^{-1}) = \frac{\beta - \beta \cdot z^{-1}}{T + T \cdot (2 \cdot \sqrt{\beta} - 2) \cdot z^{-1} + T \cdot (1 - 2 \cdot \sqrt{\beta} + \beta) \cdot z^{-2}} \quad (4.18)$$

T : sampling time

β : a coefficient which can determine the cut-off frequency of the $\alpha - \beta$ filter

$D_1(z)$ is the low-pass filter transfer function multiplied by the inverse plant transfer function (The inverse plant transfer function in the $D_1(z)$ is from velocity to voltage). We use pole-zero matched method to design $D_1(z)$.

$$D_1(z^{-1}) = \frac{B \cdot (1 - e^{(-T/\tau)})^2}{k_t \cdot k_a \cdot (1 - e^{(-B \cdot T/J)})} \cdot \frac{(z^{-1} - e^{(-B \cdot T/J)}) \cdot z^{-2}}{(1 - 2 \cdot e^{(-T/\tau)} \cdot z^{-1} + e^{(-2T/\tau)} \cdot z^{-2})} \quad (4.19)$$

$$\tau = \frac{1}{2 \cdot \pi \cdot B_w} \quad (4.20)$$

B_w :low-pass filter cut-off frequency (Hz)

$D_3(z)$ is the low-pass filter that is identical to the one in $D_1(z)$.

$$D_3(z^{-1}) = \frac{(1 - e^{(-T/\tau)})^2}{2} \cdot \frac{(z^{-1} + z^{-2})}{(1 - 2 \cdot e^{(-T/\tau)} \cdot z^{-1} + e^{(-2T/\tau)} \cdot z^{-2})} \quad (4.21)$$

$C_v(z)$ in the velocity loop is PI control.

$$C_v(z^{-1}) = k_{vp} + \frac{k_{vi} \cdot T}{1 - z^{-1}} \quad (4.22)$$

Now we will get the plant transfer $P(z)$ includes zero-order hold. See figure 4.6.

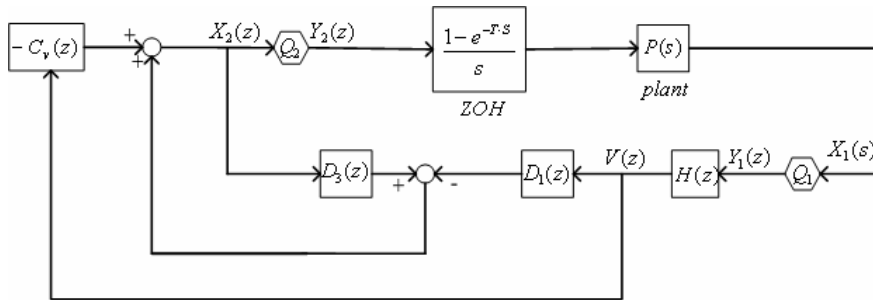


Figure 4.6 Velocity loop of the controller structure in the figure 4.1

Take the z-transform of the signal $X_1(s)$:

$$X_1(s) = \frac{1 - e^{-T \cdot s}}{s} \cdot \frac{k_a \cdot k_t}{s \cdot (J \cdot s + B)} \cdot Y_2(z^{-1})$$

$$X_1(z^{-1}) = Z \left[\frac{k_a \cdot k_t}{s^2 \cdot (J \cdot s + B)} \right] \cdot (1 - z^{-1}) \cdot Y_2(z^{-1})$$

$$\begin{aligned}
X_1(z^{-1}) &= \frac{k_t \cdot k_a \cdot J}{B^2} \cdot \frac{(B \cdot T/J - 1 + e^{-B \cdot T/J}) \cdot z^{-1} + (1 - e^{-B \cdot T/J} - B \cdot T/J \cdot e^{-B \cdot T/J}) \cdot z^{-2}}{1 - (1 + e^{-B \cdot T/J}) \cdot z^{-1} + e^{-B \cdot T/J} \cdot z^{-2}} \cdot Y_2(z^{-1}) \\
P(z^{-1}) &= \frac{k_t \cdot k_a \cdot J}{B^2} \cdot \frac{(B \cdot T/J - 1 + e^{-B \cdot T/J}) \cdot z^{-1} + (1 - e^{-B \cdot T/J} - B \cdot T/J \cdot e^{-B \cdot T/J}) \cdot z^{-2}}{1 - (1 + e^{-B \cdot T/J}) \cdot z^{-1} + e^{-B \cdot T/J} \cdot z^{-2}} \quad (4.23)
\end{aligned}$$

Now, we can take the discrete transfer functions (4.18), (4.19), (4.21), (4.22), and (4.23) into the inequality(4.16) to find appropriate parameters. The main idea is that since the parameters of J , B , k_t , k_a are dependent on the nature of the system, the parameters we need to find and adjust for absence of limit cycles are only k_{vp} , k_{vi} , β , and B_w . Let the limit cycles that occur in the system be a length (period) of 50 ($N = 50$. The larger the N is, the more stringent the inequality(4.16) is.) sample times, and the sample rate is 2 KHz ($T = 0.0005(s)$). The original parameters with limit cycles, and those for absence of limit cycles, found by utilizing the inequality (4.16) are compared in the table 4.1.

Table 4.1 The parameters for the cascade control and the parameters for the absence of limit cycles

Symbol and name	The parameters for the cascade control	The parameters for absence of limit cycles	Unit
J , inertia	2.49	2.49	Kg
B , viscous friction coefficient	44.14	44.14	kg/sec
k_{vp}	184	0.025	Volt • sec/m
k_{vi}	35537	1	Volt /m
B_w , low-pass filter cut-off freq	10	1	Hz
β	0.32	0.001	(none)
K_t , force constant of motor	28.5	28.5	N/A
K_a , gain of current driver	0.349	0.349	A/Volt
T , sampling time	0.0005	0.0005	sec

From above results, we get that the parameters need to be tuned to satisfy inequality

(4.16) is k_{vp} , k_{vi} , β , and B_w . We are aware that the value of the parameters for absence of the limit cycles is much smaller than the original one, and the system designed under these parameters has poor performance. So, in next section we will suggest an adaptive mechanism taking place after acceleration-deceleration period, to keep the system performance in transient and also avoid the limit cycle in steady state. Besides, the simple method that only reduces the cut-off frequency B_w of the low-pass filter in the disturbance observer, without tuning the parameters k_{vp} , k_{vi} of the PI controller in the velocity loop and β of the $\alpha - \beta$ filter, is not able to satisfy the inequality (4.16), also generates limit cycles in the experimental results, but with smaller amplitude and lower frequency.

4.4 Adaptive parameters mechanism:

According to the parameters we found by conforming to the inequality (4.16) in the last section, the performance in the velocity loop is too poor to meet the performance demand of the modern motion control system. In this section, we will introduce an adaptive method taking place after the acceleration-deceleration mechanism in the regulating control. The purpose of the adaptive parameters mechanism is to maintain the original designed parameters for high performance demand within acceleration-deceleration period in the velocity loop. After the period, the system will gradually become steady-state, therefore, we can linearly tune the parameters into the values for the absence of the limit cycles without severely impacting the overall performance of the system, and linearly increase the P gain in the position loop to make the system rapidly reach to the desired position. The reason for increasing the P gain in the position loop is explained as follow. After

acceleration-deceleration mechanism, the system is almost in the steady-state. The velocity of the system is very slow in this phase, so the disturbance observer making the system become nominal plant will actually take effect, and in addition, the feed-forward controller $F_v(s)$ whose design is based on the nominal plant will make the transfer function from velocity command $u_v(s)$ to velocity response $v(s)$ become one (see figure 4.1). The block diagram can be simplified as figure 4.7.

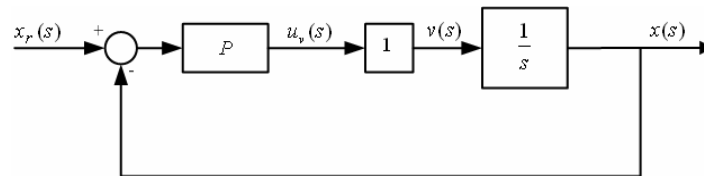


Figure 4.7 Equivalent controller structure after acceleration-deceleration period.

The system plant becomes $\frac{1}{s}$ and has a P control in the position loop. Thus, increasing the P gain will make the system quickly move to the desired position and decrease the steady-state error. The linear adaptive mechanism after the acceleration-deceleration period will be listed as below:

$$\begin{cases} \rho_i & 0 \leq t < T_{acc} \\ \rho_i - \frac{(\rho_i - \rho_f) \cdot (t - T_{acc})}{\Delta T_{tune}} & T_{acc} \leq t \leq T_{acc} + \Delta T_{tune} \\ \rho_f & t > T_{acc} + \Delta T_{tune} \end{cases} \quad (4.24)$$

ρ_i : The parameters before tuning.

ρ_f : The parameters after tuning.

T_{acc} : The acceleration-deceleration period in the regulating control (for example,

T_{acc} in figure 4.2 is the period within 0~0.25 second).

ΔT_{tune} : The period of tuning parameters (for example, ΔT_{tune} in figure 4.2 is the

period after 0.25 second).

The time for tuning parameters we recommend here is 0.5 second ($\Delta T_{tune} = 0.5$).

The parameters need to be tuned and their values before and after tuning are listed in the table 4.2.

Table 4.2 The parameters need to be tuned for the absence of limit cycles

Symbol and name	The parameters values before tuning	The parameters values after tuning
k_{pp} , P gain in the position loop	25	2000
k_{vp} , P gain in the velocity loop	184	0.025
k_{vi} , I gain in the velocity loop	35537	1
B_w , Low-pass filter cut-off freq	10	1
β	0.32	0.001

4.5 Experimental results:

We give a position command to execute the acceleration-deceleration mechanism first and then fix the system at the stationary position. The experiments will be conducted for three cases to verify the validity of the parameters for the absence of the limit cycles and the effect of the adaptive mechanism. (1). $5 \times 10^{-2}(m)$ regulating control. (2). $1 \times 10^{-3}(m)$ regulating control. (3). $1 \times 10^{-6}(m)$ regulating control.

The position command is briefly listed as below.

$$x_r(t) = \begin{cases} A \left[6 \left(\frac{t}{T_r} \right)^5 - 15 \left(\frac{t}{T_r} \right)^4 + 10 \left(\frac{t}{T_r} \right)^3 \right] & , 0 \leq t \leq T_{acc} \\ A & , t > T_{acc} \end{cases} \quad (4.25)$$

The index we use to analyze the system performance is listed as follow:

$$E_{tr} = \sqrt{\frac{1}{N} \sum_N (x_r - x)^2} \quad \text{for } 0 \leq t \leq t_r \quad (4.26)$$

$$E_{qs} = \sqrt{\frac{1}{N} \sum_N (x_r - x)^2} \quad \text{for } t_r < t \leq t_{qs} \quad (4.27)$$

$$E_{ss} = \sqrt{\frac{1}{N} \sum_N (x_r - x)^2} \quad \text{for } t_{qs} < t \leq t_{ss} \quad (4.28)$$

E_{tr} is the rms index which can be used to analyze the transient performance within the acceleration-deceleration period. E_{qs} is the rms index which can be used to analyze the system performance of converging the desired position. E_{ss} is the rms index which can be used to analyze the steady-state performance and judge whether the system can reduce the limit cycles.

(1). Large scale regulating control:

$$A = 5 \times 10^{-2} (m)$$

$$T_{acc} = 5(\text{sec})$$

E_{tr} for $0 \leq t \leq 5(\text{sec})$, E_{qs} for $5 \leq t \leq 7.5(\text{sec})$, E_{ss} for $7.5 \leq t \leq 15(\text{sec})$.

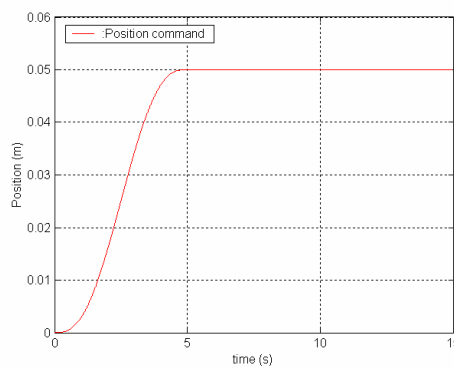


Figure 4.8 The position command in large position regulating control.

Table 4.3 Performance index of the three controller structure

Controller structure	E _{tr} (m)	E _{qs} (m)	E _{ss} (m)
1.TC(tradition controller)	1.0296×10^{-6}	2.9772×10^{-7}	4.0685×10^{-8}
2.TC+FC+DOB(without adaptive)	4.3558×10^{-7}	2.5510×10^{-7}	1.8315×10^{-7}
3.TC+FC+DOB(with adaptive)	4.2532×10^{-7}	1.1481×10^{-7}	2.3806×10^{-8}

Remark: The tradition controller (TC) is the controller structure that is identical to the one in figure 4.1 but without disturbance observer and feed-forward type friction compensator.

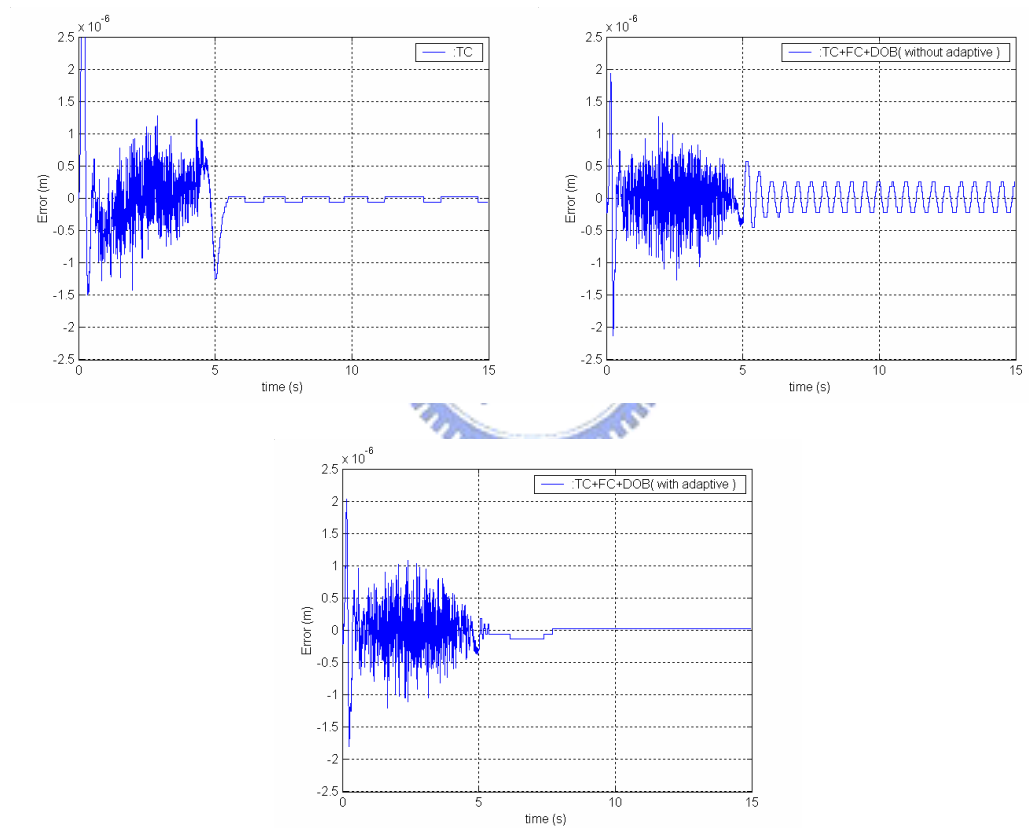


Figure 4.9 The position errors of the three controller structures in large scale regulating control

The encoder resolution we use in the large scale regulating control is $0.0791 (\mu\text{m})$.

From table 4.3, we can see that the transient performance of the controller structure 2 increases by almost 57% as compared with the controller structure 1 (TC), but it has

the worst performance in steady-state because it generates the limit cycles.

The controller structure 3 has good transient performance as well as the controller structure 2, but with the adaptive mechanism, the performance of converging desired position (E_{qs}) and steady-state (E_{ss}) is superior to the controller structure 2 and is the best of the all three controller structure. As we can see, the limit cycles in the controller structure 2, caused by the mutual effect between the disturbance observer and the quantization, are the pure harmonic limit cycles (no dc components), so the assumption in section 2 makes sense. The limit cycles of the controller structure 1 (TC) within 5~15 (sec) are not identical with the limit cycles of the controller structure 2. The desired position $5 \times 10^{-2}(m)$ of the position command cannot be divided by the encoder resolution $7.91 \times 10^{-8}(m)$ with no remainder, so there is always an offset error of the position. Therefore, the behavior to continue correcting the offset error in the feedback loop cause the limit cycles of the controller structure 1 which has only one count drift. The controller structure 3 is not sensitive to the offset error because we decrease the gain of the velocity loop controller $c_v(s)$ to a very low value.

(2).Medium scale regulating control:

$$A = 1 \times 10^{-3}(m)$$

$$T_{acc} = 0.25(\text{sec})$$

$$E_{tr} \text{ for } 0 \leq t \leq 0.25(\text{sec}), E_{qs} \text{ for } 0.25 \leq t \leq 2.5(\text{sec}), E_{ss} \text{ for } 2.5 \leq t \leq 15(\text{sec}).$$

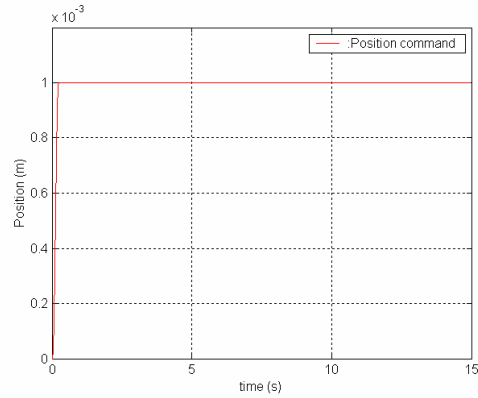


Figure 4.10 The position command in medium position regulating control

Table 4.4 Performance index of the four controller structure

Controller structure	Etr (m)	Eqs(m)	Ess (m)
1.TC(tradition controller)	6.0971×10^{-6}	4.9790×10^{-7}	3.5595×10^{-8}
2.TC+FC+DOB(without adaptive)	1.4605×10^{-6}	3.5158×10^{-7}	2.3249×10^{-7}
3.TC+FC+DOB(only lower B_w)	1.7968×10^{-6}	3.5505×10^{-7}	5.6946×10^{-8}
4.TC+FC+DOB(with adaptive)	1.4448×10^{-6}	1.6204×10^{-7}	3.3081×10^{-8}

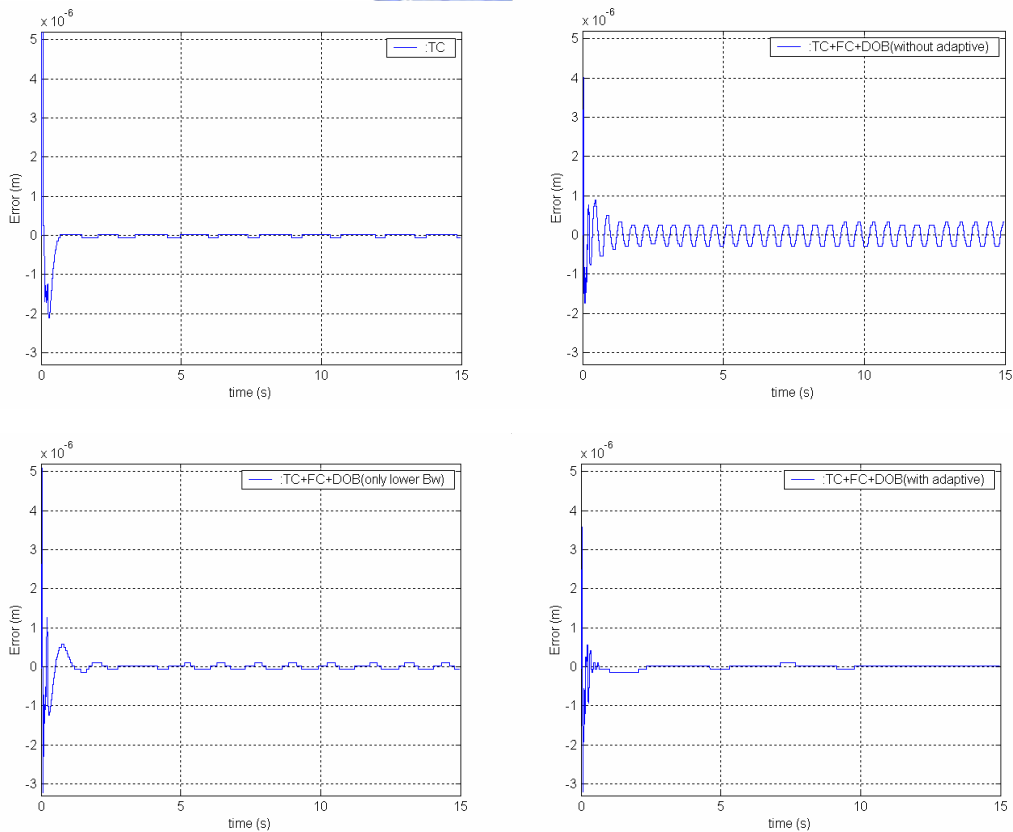
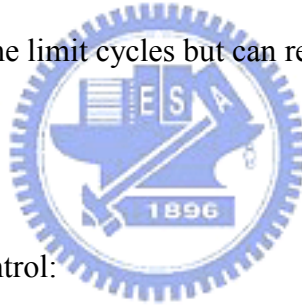


Figure 4.11 The position errors of the four controller structure in medium scale regulating control

The encoder resolution we use in the medium scale regulating control is $0.0791 (\mu m)$. The results in the medium scale regulating control is similar to the results in the large scale. The controller structure 4 with adaptive mechanism has the best overall performance. The transient performance of the controller structure 4 is as good as the controller structure 2,3, and increases by 76% as compared with the controller structure 1. Furthermore, the performance of converging to the desired position of the controller structure 4 is almost 2 times better than the other three and the steady-state error (E_{ss}) also decreases by 85% as compared with the controller structure 2 without the adaptive mechanism. As we can see from figure 4.11, the controller structure 3 only with lowered the cut-off frequency B_w of the low-pass filter can't completely avoid the limit cycles but can reduce the amplitude and frequency of the limit cycles.



(3). Micro scale regulating control:

$$A = 1 \times 10^{-6} (m)$$

$$T_{acc} = 0.25(\text{sec})$$

$$E_{tr} \text{ for } 0 \leq t \leq 0.25(\text{sec}), E_{qs} \text{ for } 0.25 \leq t \leq 2(\text{sec}), E_{ss} \text{ for } 2 \leq t \leq 12(\text{sec}).$$

Table 4.5 Performance index of the three controller structure

Controller structure	E _{tr} (m)	E _{qs} (m)	E _{ss} (m)
1.TC(tradition controller)	3.0239×10^{-7}	7.1596×10^{-8}	1.7378×10^{-8}
2.TC+FC+DOB(without adaptive)	2.3928×10^{-7}	8.5135×10^{-8}	3.8542×10^{-8}
3.TC+FC+DOB(with adaptive)	1.0317×10^{-7}	2.4583×10^{-8}	2.2608×10^{-8}

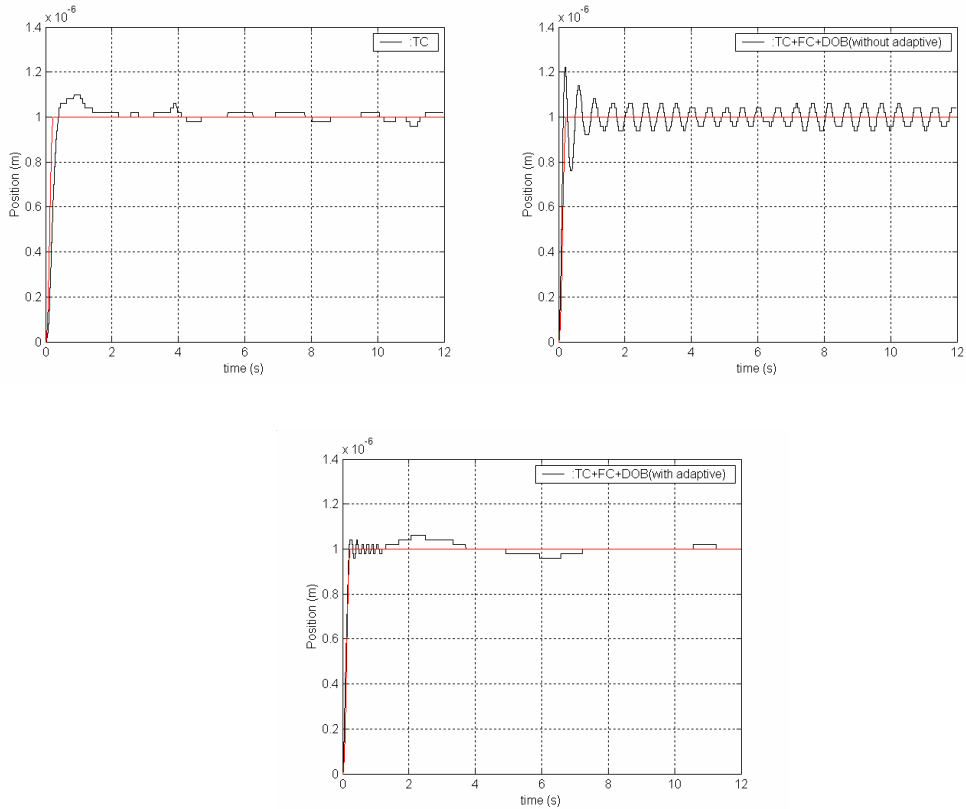


Figure 4.12 The position response of the three controller structures in micro scale regulating control



The encoder resolution we used in the micro scale regulating control is $0.02 (\mu m)$.

The controller structure 3 with adaptive mechanism has the best performance in terms of E_{tr} and E_{qs} . Although the steady-state performance of the controller structure 3 is worse than the controller structure 1, it is still much better than the controller 2 by reducing the limit cycles.

4.6 Summary:

In this article, we introduce a sufficient condition of eliminating the limit cycles induced by the disturbance observer and quantization. The sufficient condition enables us to design appropriate parameters in the velocity loop to avoid the limit cycles. However, we are not satisfied about the performance of the parameters

which conforms to the sufficient condition. We further introduce a linear adaptive mechanism that not only maintains the transient performance but also reduces the limit cycles in the steady-state. As we can see from the experimental results in section 4.5, the TC+FC+DOB control structure with the adaptive mechanism has the best overall performance in regulating control.



Chapter 5

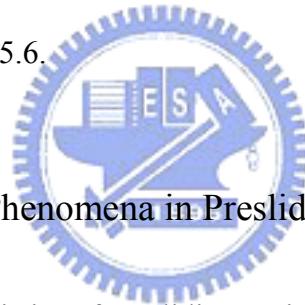
The Modified Friction Model for Motion Control in Presliding Region

5.1 Introduction:

In mechanical system friction is complex and highly nonlinear phenomenon. Friction deteriorates the tracking performance, especially in presliding region, and generates anxiety limit cycle in regulating control. In order to propose an elaborate friction model as a tool to design a friction estimator and predict nonlinear phenomena, we need to understand more about friction phenomenon. The most common model for control purpose is LueGre model proposed by C.Canudas de Wit [8] in 1995. This model can capture the characteristics between presliding region and sliding region without any switching function, using the LueGre model to design a friction compensator is easy. However, in the presliding region the LueGre model cannot capture some important phenomena like hysteresis loop with non local memory, memory wipe out and nonlinear spring after velocity reversal [62], [26], [19]. Consequently, we are not able to obtain satisfied control performance based on LueGre model in presliding region. After LueGre model was announced, Jan Swevers [62] modified this model into an integrated friction model using multi-state technique to capture hysteresis loop with non local memory and memory wipe out

phenomenon. Nevertheless, this model did not have an appropriate transition curve (i.e., a function that describe the relationship between friction force and bristles displacement) to capture the nonlinear spring characteristic after velocity reversal. In this chapter we will introduce a nonlinear function that suitably describes the nonlinear spring characteristic and is easy to implement for motion control.

The sections of this chapter will be organized as below: Firstly, in section 5.2, we would present some important friction phenomena in presliding region, point out the shortcomings of LueGre model and further propose the modified friction model in the section 5.3. Next, the procedure of identifying modified friction model's parameters is introduced in section 5.4. In section 5.5, to verify the accuracy of the modified model, we use this model to compensate friction in linear motor system. Finally, the conclusion is given in section 5.6.



5.2 Important Friction Phenomena in Presliding Region:

There are some characteristics of presliding region that are obviously observed in experiments. We will list those characteristics and explain them in detail as follows: (a) elastic-plastic like deformation. (b) hysteresis loop with non local memory and memory wipe out. (c) nonlinear-spring phenomenon after velocity reversal.

(a) Elastic-plastic like deformation:

Between the two contacting surfaces in the presliding region, it is considered that a lot of bristles are randomly distributed and act as spring characteristic. When relative motion between two surfaces is made, the spring will have deformation and generate opposite force to counteract the motion. This opposite force is analogous to friction force (figure 5.1).



Figure 5.1 Bristles model.

Initially, the bristles adhere to the surface, so the spring's deformation rate is equal to relative velocity between two surfaces. As the surfaces continue to move, the bristles start to slip. Therefore, the deformation rate of the spring becomes slower than relative velocity, and then the spring ceases deformation while it is slipping completely. After that, the lubricant starts to form, and the system enters sliding (macro) region where Stribeck effects, Coulomb friction and viscous friction are the main characteristics (see figure 5.2).

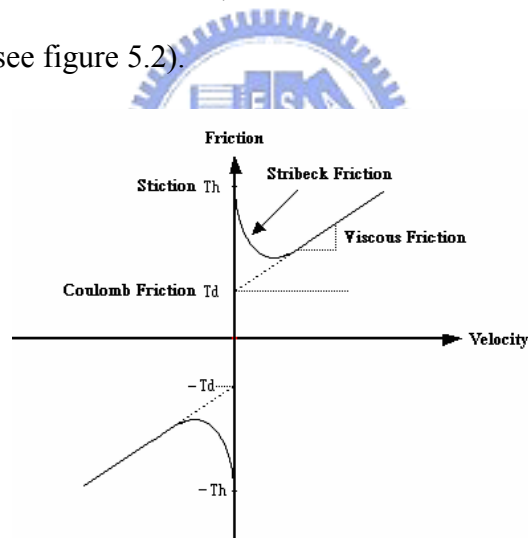


Figure 5.2 Friction characteristics in sliding region

The phenomenon described above can be thought as elastic-plastic like deformation. The elastic term that contributes friction force is analogous to the spring deformation, and the plastic term that does not contribute friction force is equal to the bristles' slip phenomenon we mentioned above. Consequently, relative motion between two surfaces only causes elastic (spring) deformation initially, but as the motion goes, it causes not only elastic deformation but also plastic deformation. The spring finally

has breakaway (completely slip), and the system transits to sliding (macro) region. LueGre model has this property. It uses the z state to represent the elastic deformation and has an implicit state to represent the plastic deformation.

(b) Hysteresis loop with non local memory and memory wipe out:

In presliding region the friction force depends much on displacement, the relationship between friction and displacement is quite important. One of the most important relationships between friction force and displacement in presliding region is hysteresis loop with non local memory and memory wipe out. We will explain this characteristic as below. If one of the velocities of the system changes its direction (maybe from positive velocity to negative velocity, or from negative velocity to positive velocity), a velocity reversal happens, and the point where the system changes its velocity direction is called “turning point”. After this point, the friction-displacement curve will generate new branch (see figure 5.3).

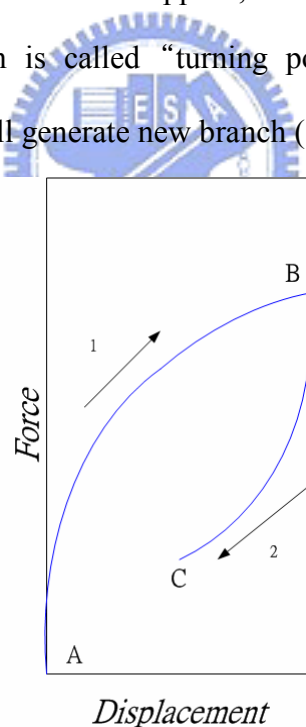


Figure 5.3 System has velocity reversal at turning point B and generate a new friction-displacement curve ($B \rightarrow C$).

When any friction-displacement curve which has tendency to go back to the last turning point passes through the last turning points, there forms a closed friction-displacement curve called “hysteresis loop” (see figure 5.4).

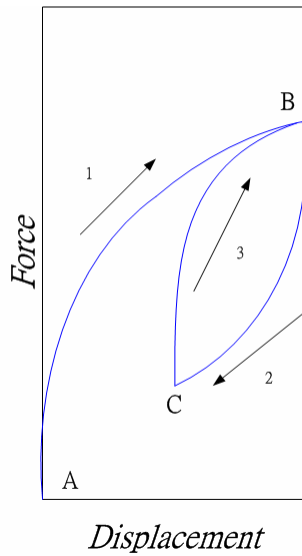


Figure 5.4 Curve $(C \rightarrow B)$ has tendency to go back to its last turning point B and there finally forms a hysteresis loop $(B \rightarrow C \rightarrow B)$.

If a friction-displacement curve goes after this hysteresis loop, its tendency or shape will not follow the former friction-displacement curve that forms this hysteresis loop and may follow the earlier generated curve that is not part of this hysteresis loop (see figure 5.5)

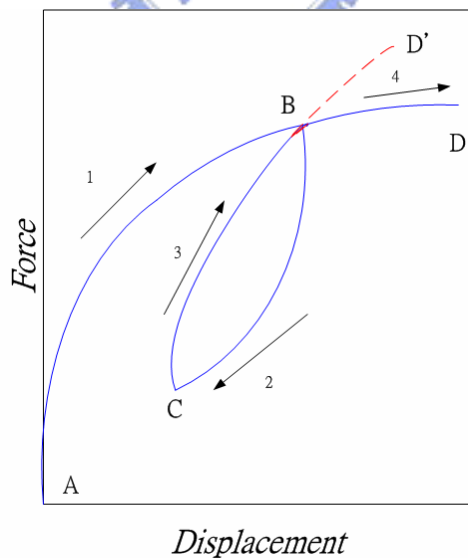


Figure 5.5 The friction-displacement curve $(B \rightarrow D)$ doesn't follow the curve $(C \rightarrow B)$ but follow the curve $(A \rightarrow B)$ which is generated earlier than the curve $(C \rightarrow B)$.

The phenomenon described above is “memory wipe out” . One can imagine that

the hysteresis loop immediately vanishes from our memory after it is formed, so any curve that goes afterwards is not influenced by this loop and may follow the earlier generated curve that isn't part of this loop. The term “non local memory” is similar to the term “memory wipe out”, which means that the friction-displacement curve’s tendency is not only influenced by early curve but also by extremely earlier curve. The best example was illustrated in figure 5.5 where curve ($B \rightarrow D$) follows from extremely earlier curve ($A \rightarrow B$) not curve ($C \rightarrow B$). LueGre model can’t capture the phenomenon we have described above, but Jan Swevers’s integrated friction model can.

(c) Nonlinear-spring phenomenon after velocity reversal:

In Futami research [19], the author finds out that a nonlinear spring phenomenon appears after the system has velocity reversal. The main characteristics of the nonlinear spring is that the spring’s stiffness is very high after velocity reversal, but the stiffness will decline gradually as the system is moving away from the turning point (see figure 5.6).

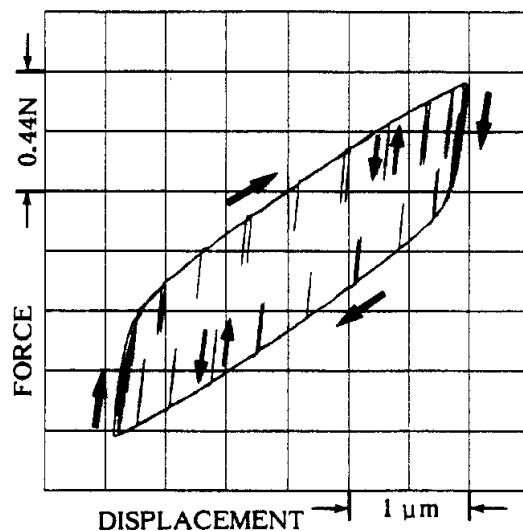


Figure 5.6 Outline of force-to-displacement relationship of a ball screw driven slider (Futami *et al.*, 1990 [19]).

So the friction-displacement curve’s slope (spring stiffness) is very steep initially after

the system occurs velocity reversal and will gradually become less steep as displacement is increasing. Jan Swevers did not introduce an appropriate friction function of elastic deformation $f(z)$ to describe this phenomenon. We will use an appropriate nonlinear spring function $f(z)$ to describe this in next section.

5.3 LueGre model and Modified friction model:

LueGre model is briefly listed as below.

$$\frac{dz}{dt} = v - \frac{|v|}{g(v)} \cdot \sigma_0 \cdot z \quad (5.1)$$

$$F = \sigma_0 \cdot z + \sigma_1 \cdot \frac{dz}{dt} + B \cdot v \quad (5.2)$$

$$g(v) = F_c + (F_s - F_c) \cdot e^{-\frac{|v|}{v_s}} \quad (5.3)$$

where z is the bristles' deformation; σ_0 is the spring's stiffness; σ_1 is the micro's viscous coefficient; B is the macro's viscous coefficient; v is the system's velocity; F_s is the stick force; F_c is the Columb friction force; $g(v)$ is the positive function that can describe the Stribeck effect, and Columb friction in sliding region. The right term $\frac{|v|}{g(v)} \cdot \sigma_0 \cdot z$ in equation (5.1) is thought as plastic deformation rate. The system velocity v minus plastic deformation rate leaves elastic deformation rate.

So $\frac{dz}{dt}$ can be considered as elastic deformation rate. Equation (5.1) can describe the elastic-plastic like deformation we have described in the last section. To explain this, let's give an example of a system moving at positive velocity. At the beginning of the motion, there is no bristles' deformation ($z=0$), so the rate of the plastic deformation is also zero. Consequently, $\frac{dz}{dt} = v - \frac{|v|}{g(v)} \cdot 0 = v$. Only elastic deformation happens initially, but as the system moves further, there also has plastic deformation. As motion goes, the elastic deformation

rate $\left(\frac{dz}{dt} = v - \frac{|v|}{g(v)} \cdot \sigma_0 \cdot z < v \text{ for } v > 0, z > 0\right)$ is getting less than the system's velocity. The elastic part of the bristles stops deformation when the value of the term $\sigma_0 \cdot z$ reaches the positive function $g(v)$ that can describe sliding region phenomenon.

At the moment, $\frac{dz}{dt} = v - \frac{|v|}{g(v)} \cdot \sigma_0 \cdot z = v - \frac{|v|}{g(v)} \cdot g(v) = 0$. Equation (5.2) can be rewritten as bellow:

$$F = g(v) + B \cdot v. \quad (5.4)$$

The elastic deformation transits into steady state, and we can call “The bristle has breakaway”. According to equation (5.4), the physical characteristics of friction switch from presliding region into sliding region. As mentioned above, LueGre model can adequately describe the elastic-plastic like deformation but can't actually describe hysteresis loop with non local memory, memory wipe out phenomenon. Jan Swevers modified the plastic deformation term of LueGre model and used a multi state technique to overcome this deficiency in LueGre model. Before we discuss the reason why Jan Swevers' integrated friction model can describe this phenomenon, let's introduce this model first. This model is listed as below:

$$\frac{dz}{dt} = v - \frac{v}{s(v) - f_r} \cdot f_d(z) \quad (5.5)$$

$$F = f_r + f_d(z) + \sigma_1 \cdot \frac{dz}{dt} + B \cdot v \quad (5.6)$$

$$s(v) = \text{sgn}(v) \cdot [F_c + (F_s - F_c) \cdot e^{-\frac{|v|}{v_s}}] \quad (5.7)$$

where f_r is the friction force at turning point (the point where the system has velocity reversal), $f_d(z)$ is the transition curve (the function that describes the relationship between friction and elastic deformation), $s(v)$ is similar to the $g(v)$ in the LueGre model. The only difference between them is that $s(v)$ has to multiply by $\text{sgn}(v)$. So $s(v)$ is not always a positive function like $g(v)$, it will

change between positive or negative function according to the system's velocity. f_r , $f_d(z)$ are not always unchanged, whereas they change according to some rules.

Before we list these rules, we now present a new thing called "memory stack".

Memory stack is a stack that stores information of turning points and is important for the integrated friction model. Initially, it stores the information of starting point and will add or eliminate information of turning points according to the rules as below:

Rule 1): If one system has new turning point (velocity reversal), f_r in equation (5.5) will change from the old turning point's friction force to the new turning point's friction force and add the new turning point's information to the memory stack from top of it and resets $f_d(z)$ to zero, so the transition curve $f_d(z)$ after the new turning point will start from zero (see figure 5.7 and 5.8).

Memory stack (after initial point p_0):

$$[f_{r0}]$$

equation(5.5) (after initial point p_0):

$$\frac{dz}{dt} = v - \frac{v}{s(v) - f_{r0}} \cdot f_{d0}(z)$$

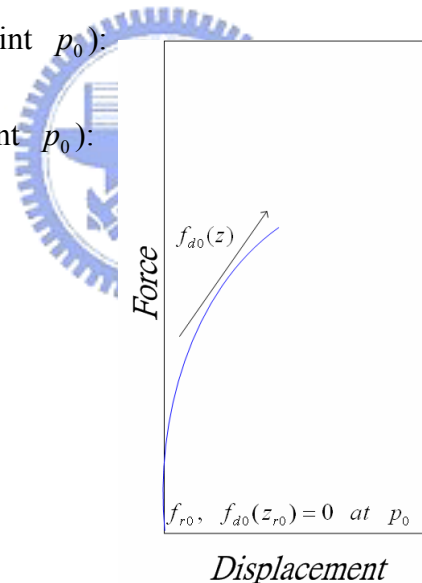


Figure 5.7 Status of memory stack and equation (5.5) after initial turning point p_0 .

Memory stack (after turning point p_1):

$$\begin{bmatrix} f_{r1} \\ f_{r0} \end{bmatrix}$$

Equation(5.5) (after turning point p_1):

$$\frac{dz}{dt} = v - \frac{v}{s(v) - f_{r1}} \cdot f_{d1}(z)$$

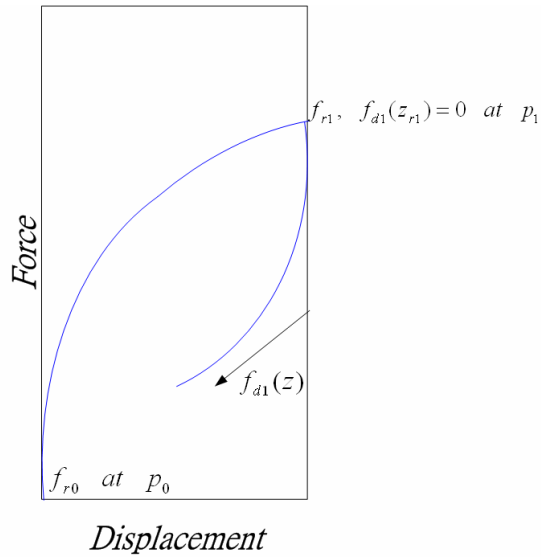


Figure 5.8 Status of memory stack and equation (5.5) after turning point p_1 .

Rule 2): The friction-displacement transition curve has tendency to pass through the last turning point and forms a hysteresis loop. When it forms a hysteresis loop, we must update the memory stack to execute the operation called “memory wipe out” .

There are two update laws of the “memory wipe out” , which is dependent on the size of the memory stack.

2-1): If the amount of the turning point information in the memory stack exceeds two, we clean up the top two turning point in the memory stack. After cleaning up the memory stack, set the top one as the current turning point information. The value of $f_d(z)$ doesn't need to be set to zero, but its tendency or shape afterward will change to follow from (or be influenced by) top turning point in the memory stack which has been cleaned up (see figure 5.9 and 5.10).

Memory stack:

$$\begin{bmatrix} f_{r2} \\ f_{r1} \\ f_{r0} \end{bmatrix}$$

Equation (5.5):

$$\frac{dz}{dt} = v - \frac{v}{s(v) - f_{r2}} \cdot f_{d2}(z)$$

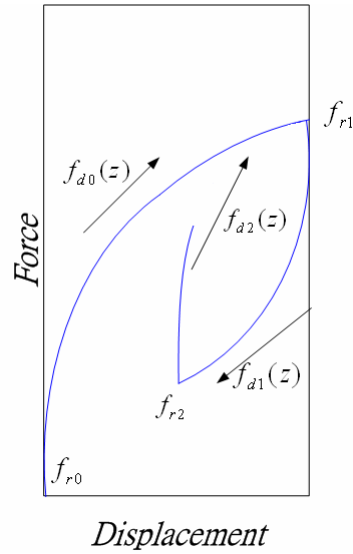


Figure 5.9 Status of memory stack and equation (5.5) before the friction-displacement transition curve completes the hysteresis loop.

Memory stack:

$$[f_{r0}]$$

Equation (5.5):

$$\frac{dz}{dt} = v - \frac{v}{s(v) - f_{r0}} \cdot f_{d0}(z)$$

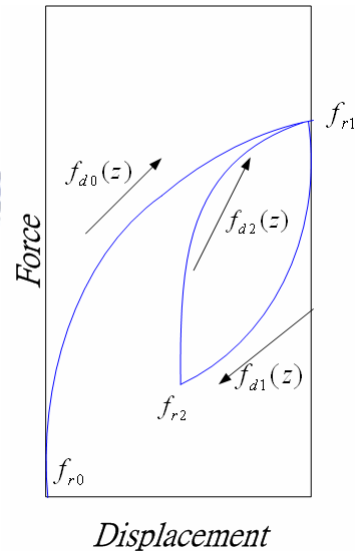


Figure 5.10 Status of memory stack and equation (5.5) after the friction-displacement transition curve completes the hysteresis loop.

2-2): If there are only two turning points information in the memory stack, set the bottom turning point information equal to the top one. Then, clean up the top turning point information and set the bottom one as current turning point information. The value of $f_d(z)$ doesn't need to be set to zero, and its tendency or shape afterward will remain unchanged (see figure 5.11, 5.12).

Memory stack:

$$\begin{bmatrix} f_{r1} \\ f_{r0} \end{bmatrix}$$

Equation (5.5):

$$\frac{dz}{dt} = v - \frac{v}{s(v) - f_{r1}} \cdot f_{d1}(z)$$

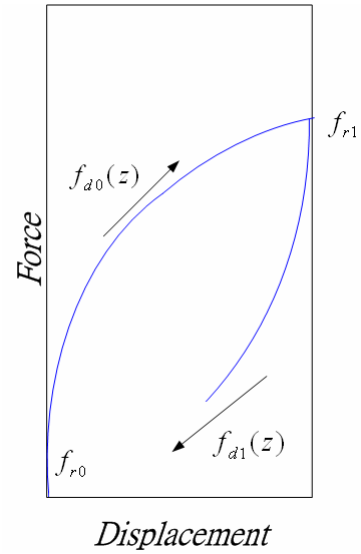


Figure 5.11 Status of memory stack and equation (5.5) before the friction-displacement transition curve completes the hysteresis loop.

Memory stack:

$$[f_{r0} = f_{r1}]$$

Equation(5.5):

$$\frac{dz}{dt} = v - \frac{v}{s(v) - f_{r0}} \cdot f_{d1}(z)$$

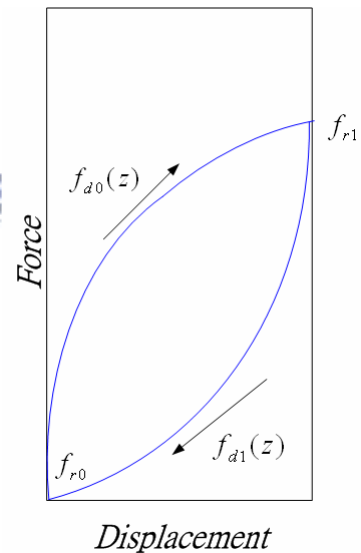


Figure 5.12 Status of memory stack and equation (5.5) after the friction-displacement transition curve completes the hysteresis loop.

Now we start to explain why LueGre model can not capture hysteresis loop with non local memory and memory wipe out phenomenon. First, we obtain the relationship between solid friction force and displacement, which is implied implicitly in LueGre model.

Let solid friction term as follow:

$$F_{solid} = \sigma_0 \cdot z \quad (5.8)$$

Differentiate solid friction with respect to displacement:

$$\frac{dF_{solid}}{dx} = \sigma_0 \cdot \frac{dz}{dx} \quad (5.9)$$

$$\frac{dF_{solid}}{dx} = \sigma_0 \cdot \left(1 - \frac{\text{sgn}(v)}{g(v)} \cdot F_{solid}\right) \quad (5.10)$$

As we can see, equation (5.10) indicates the relationship between solid friction force and displacement. LueGre model has some shortcoming in presliding region and we will use equation (5.10) to show them by a simple example (note: In the following example, the value of solid friction F_{solid} is represented in the form of stick friction F_s multiplied by some value, for example, $0.5 \cdot F_s$, $0.25 \cdot F_s$, ...etc, and $g(v) = F_s$ because all of the examples is in the presliding region).

Example 1): If one system's motion does not exceed presliding region, and its friction-displacement transition curve is illustrated in figure 5.13. The initial value of $\left. \frac{dF_{solid}}{dx} \right|_{p_1}$ after turning point P_1 can be calculated as follow:

$$\left. \frac{dF_{solid}}{dx} \right|_{p_1} = \sigma_0 \cdot \left(1 - \frac{-1}{F_s} \cdot 0.5 \cdot F_s\right) = 1.5 \cdot \sigma_0$$

The initial value of $\left. \frac{dF_{solid}}{dx} \right|_{p_2}$ after turning point P_2 is:

$$\left. \frac{dF_{solid}}{dx} \right|_{p_2} = \sigma_0 \cdot \left(1 - \frac{1}{F_s} \cdot 0.25 \cdot F_s\right) = 0.75 \cdot \sigma_0$$

We find that the friction-displacement curve's slope after turning point P_1 is much steeper than the slope after turning point P_2 from above calculation, so the friction-displacement curve after turning point P_2 can never pass through P_1 to form a hysteresis loop.

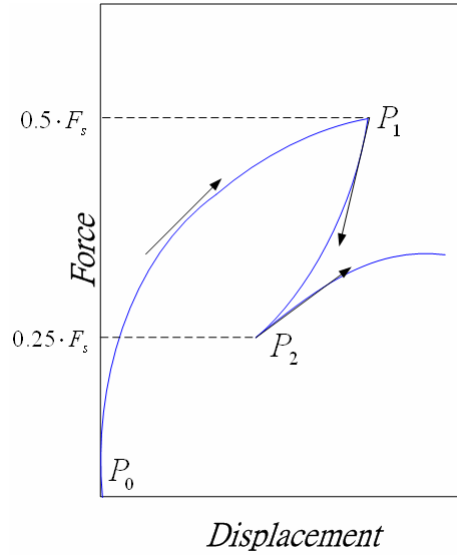


Figure 5.13 The friction-displacement transition curve caused by LueGre model.

Let's see the friction-displacement transition curve in Jan Swever's Integrated friction model. First, we derive the relationship between solid friction and displacement.

Let solid friction term as follow:

$$F_{solid} = f_r + f_d(z) \quad (5.11)$$

Differentiate solid friction with respect to displacement:

$$\frac{dF_{solid}}{dx} = \frac{df_d(z)}{dz} \cdot \frac{dz}{dx} \quad (5.12)$$

We can rewrite equation (5.5) as follow:

$$\begin{aligned} \frac{dz}{dx} \cdot \frac{dx}{dt} &= v - \frac{v \cdot f_d(z)}{s(v) - f_r} \\ \frac{dz}{dx} \cdot v &= v - \frac{v \cdot f_d(z)}{s(v) - f_r} \\ \frac{dz}{dx} &= 1 - \frac{f_d(z)}{s(v) - f_r} \end{aligned} \quad (5.13)$$

Take equation (5.13) into equation (5.12):

$$\frac{dF_{solid}}{dx} = \frac{df_d(z)}{dz} \cdot \left(1 - \frac{f_d(z)}{s(v) - f_r}\right) \quad (5.14)$$

If the relationship between friction and bristles' deformation is a simple linear spring which is similar to LueGre model and the spring's stiffness is k . Equation (5.14) can be rewritten as follow:

$$\frac{dF_{solid}}{dx} = k \cdot \left(1 - \frac{f_d(z)}{s(v) - f_r}\right) \quad (5.15)$$

Thus, equation (5.15) is the relationship between friction force and displacement.

Then, we will give example 2 to show why Jan Swever's Integrated friction model can show the hysteresis loop with non local memory characteristic.

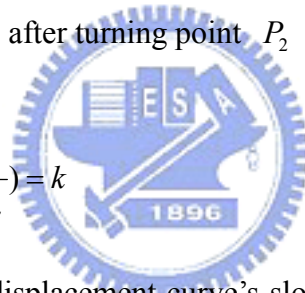
Example 2): If one system's motion doesn't exceed presliding region, and its friction-displacement transition curve is illustrated in figure 5.14, the initial value of

$\left. \frac{dF_{solid}}{dx} \right|_{P_1}$ after turning point P_1 can be calculated as follow:

$$\left. \frac{dF_{solid}}{dx} \right|_{P_1} = k \cdot \left(1 - \frac{0}{-F_s - 0.5 \cdot F_s}\right) = k$$

The initial value of $\left. \frac{dF_{solid}}{dx} \right|_{P_2}$ after turning point P_2 is:

$$\left. \frac{dF_{solid}}{dx} \right|_{P_2} = k \cdot \left(1 - \frac{0}{F_s - 0.25 \cdot F_s}\right) = k$$



We find that the the friction-displacement curve's slope caused by integrated friction model after turning point P_1 is almost as steep as the curve's slope after turning point P_2 . In details, the curve after turning point P_1 is a little bit steeper than the curve after turning point P_2 because the denominator of the negative term $-\frac{f_d(z)}{s(v) - f_r}$ in equation (5.15) after turning point P_1 is higher than the denominator after turning point P_2 .

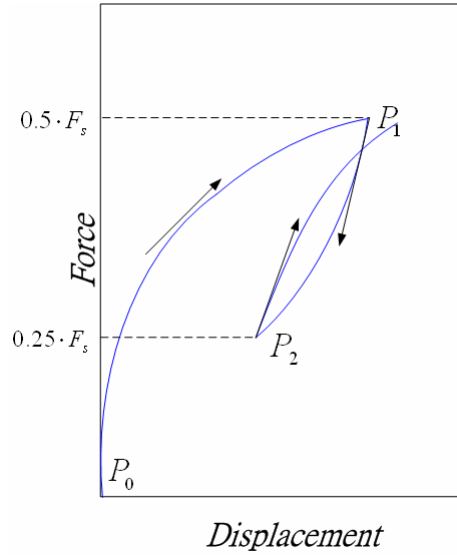


Figure 5.14 The friction-displacement transition curve caused by Jan Swevers' integrated friction model.

To conclude, the main objective of the multi state dynamic model proposed by Jan Swevers is to avoid the slope of the friction-displacement transition curve after current turning point being quite different from the friction-displacement transition curve after the last turning point. Therefore, it is possible that the transition curve passes through the last turning point and forms a hysteresis loop. The integrated friction model is much more accurate than LueGre model (which doesn't have this property) in presliding region.

Nonetheless, Jan Swevers did not introduce a suitable friction-bristles' deformation transition curve $f_d(z)$ which is convenient to implement and can certainly have the nonlinear spring phenomenon after velocity reversal. We will introduce a nonlinear spring function [26] that can capture this characteristic and is easy to implement for motion control.

This nonlinear spring function is described as bellow:

$$\frac{df}{dz} = k_1 + k_2 \cdot e^{-|z-z_r|} \quad (5.16)$$

where k_1 and k_2 is the spring's stiffness, z is the bristles' deformation, z_r is the

bristles' deformation at a turning point. As we observe from equation (5.16), a nonlinear spring's initial stiffness is $k_1 + k_2$ and its stiffness will decay exponentially to k_1 as the spring's deformation goes far from the turning point z_r . We will integrate equation (5.16) from turning point z_r to any point after z_r . Then, obtain the relationship between friction force and bristles' deformation. The integration will have two cases: 1. positive velocity. 2. negative velocity.

1. positive velocity.

$$df = k_1 \cdot dz + k_2 \cdot e^{-|z-z_r|} \cdot dz$$

$$\int_{f_r}^f df = \int_{z_r}^z (k_1 + k_2 \cdot e^{-(z-z_r)}) \cdot dz$$

$$f = f_r + k_1 \cdot (z - z_r) - \frac{1}{\beta} \cdot k_2 \cdot e^{-\beta(z-z_r)} + \frac{1}{\beta} \cdot k_2$$

where f_r is the friction force at turning point, so the friction-bristles' deformation transition curve $f_d(z)$ in positive velocity case is:

$$f_d(z) = k_1 \cdot (z - z_r) - \frac{1}{\beta} \cdot k_2 \cdot e^{-\beta(z-z_r)} + \frac{1}{\beta} \cdot k_2 \quad (5.17)$$

2. negative velocity:

$$\int_{f_r}^f df = \int_{z_r}^z (k_1 + k_2 \cdot e^{(z-z_r)}) \cdot dz$$

$$f = f_r + k_1 \cdot (z - z_r) + \frac{1}{\beta} \cdot k_2 \cdot e^{\beta(z-z_r)} - \frac{1}{\beta} \cdot k_2$$

So, the friction-bristles' deformation transition curve $f_d(z)$ in negative velocity case is:

$$f_d(z) = k_1 \cdot (z - z_r) + \frac{1}{\beta} \cdot k_2 \cdot e^{\beta(z-z_r)} - \frac{1}{\beta} \cdot k_2 \quad (5.18)$$

Now the memory stack we have introduced above must store two kind of information. One is friction force at a turning point; the other is bristles' deformation at a turning point. The information of bristles' deformation at a turning point is so convenient to us. While velocity reversal happens, we just set f_r of equation (5.5) as current

friction force and $f_d(z)$ starts by setting z_r as current bristles' deformation. Then, $f_d(z)$ will go from zero value and have high initial stiffness after a turning point in order to capture the nonlinear spring phenomenon. If a friction-displacement curve forms a hysteresis loop, we just clean up the top two data of memory stack and set z_r of $f_d(z)$ and f_r in equation (5.5) equal to the value recorded in the top information of memory stack after cleaning up. Then tendency of the curve ($f_r + f_d(z)$) after the hysteresis loop will be influenced by a extremely early curve or turning point that is not the part of the hysteresis loop, and then the curve have the hysteresis loop with non local memory characteristic. Let's take an example from figure 5.5. When the transition curve forms a hysteresis loop at turning point B, we set z_r of $f_d(z)$ and f_r in equation (5.5) after turning point B equal to bristles' deformation and solid friction force at turning point A. The curve ($B \rightarrow D$) after turning point B will follow from the curve ($A \rightarrow B$), not ($C \rightarrow B$). Therefore, the curve has the characteristic of hysteresis loop with non local memory.

The nonlinear spring function in equation (5.17) and (5.18) which can return to the last turning point is another convenient property. Therefore, with this property, to determine whether a friction-displacement curve forms a hysteresis loop becomes easy. For illustration, we take an example that a system's motion has positive velocity first, changes to negative velocity, and the curve goes back to the original point (see figure 5.15).

The value of f_{r1} can be written as follow:

$$f_{r1} = f_{r0} + k_1 \cdot (z_{r1} - z_{r0}) - \frac{1}{\beta} \cdot k_2 \cdot e^{-\beta \cdot (z_{r1} - z_{r0})} + \frac{1}{\beta} \cdot k_2 \quad (5.19)$$

The solid friction force after turning point P_1 can be written as follows:

$$\begin{aligned} f(z) &= f_{r1} + f_{d1}(z) \\ &= f_{r1} + k_1 \cdot (z - z_{r1}) + \frac{1}{\beta} \cdot k_2 \cdot e^{\beta \cdot (z - z_{r1})} - \frac{1}{\beta} \cdot k_2 \end{aligned} \quad (5.20)$$

If the curve returned to original point P_0 , $f(z)$ equaled to f_{r0} . Equation (5.20) can be written as follows:

$$f_{r0} = f_{r1} + k_1 \cdot (z - z_{r1}) + \frac{1}{\beta} \cdot k_2 \cdot e^{\beta \cdot (z - z_{r1})} - \frac{1}{\beta} \cdot k_2 \quad (5.21)$$

Take equation (5.19) into equation (5.21):

$$f_{r0} = f_{r0} + k_1 \cdot (z_{r1} - z_{r0}) - \frac{1}{\beta} \cdot k_2 \cdot e^{-\beta \cdot (z_{r1} - z_{r0})} + \frac{1}{\beta} \cdot k_2 + k_1 \cdot (z - z_{r1}) + \frac{1}{\beta} \cdot k_2 \cdot e^{\beta \cdot (z - z_{r1})} - \frac{1}{\beta} \cdot k_2$$

Solve the above equation to obtain the value of z , which make the solid friction force after turning point P_1 equal to original point P_0 's solid friction force. The solution is $z = z_{r0}$, so the curve can go back to the original point (The counterpart can be shown in the same way).

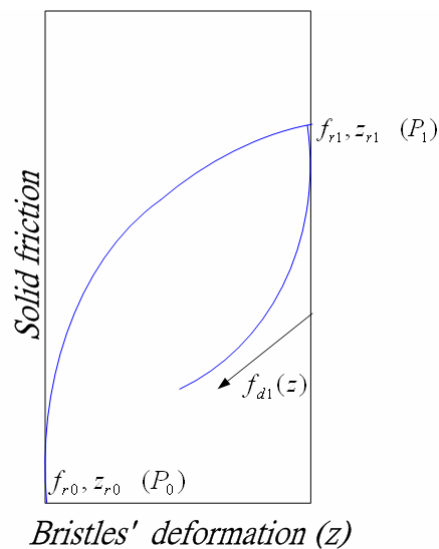


Figure 5.15 Solid friction force versus bristles' deformation

Because of the property mentioned above, the principle that can be used to determine whether a friction-displacement curve forms a hysteresis loop can be briefly listed as below.

Positive velocity case:

If the current bristles' deformation z is larger than the bristles' deformation at the last turning point, then a curve has formed a hysteresis loop.

*If $z \geq z_r[index-1]$ then
a curve has formed a hysteresis loop
end*

Negative velocity case:

If the current bristles' deformation z is smaller than the bristles' deformation at the last turning point, then a curve has formed a hysteresis loop.

*If $z \leq z_r[index-1]$ then
a curve has formed a hysteresis loop
end*

Now we will take a look at the features of the modified friction model in sliding region. While the system is entering into the sliding region, $\frac{dz}{dt}$ in equation (5.5) equals to zero.

$$v - \frac{v}{s(v) - f_r} \cdot f_d(z) = 0$$

$$\text{then, } f_r + f_d(z) = s(v)$$



$$(5.22)$$

Take equation (5.22) into equation (5.6):

$$F = s(v) + B \cdot v$$

$$(5.23)$$

According to equation (5.23), the modified friction model also has the Stribeck effect, Columb friction, and viscous friction characteristics in sliding region.

As we have discussed previously, the modified friction model could capture phenomena much more accurately than LueGre model in presliding region and the properties of the two models in sliding region are the same. The nonlinear spring function we use in the modified friction model make this model easy to implement and could certainly capture the phenomenon in reality. In the end of this section, we will use a block diagram to illustrate the procedure of estimating friction by the modified friction model in real-time system (see figure5.16).

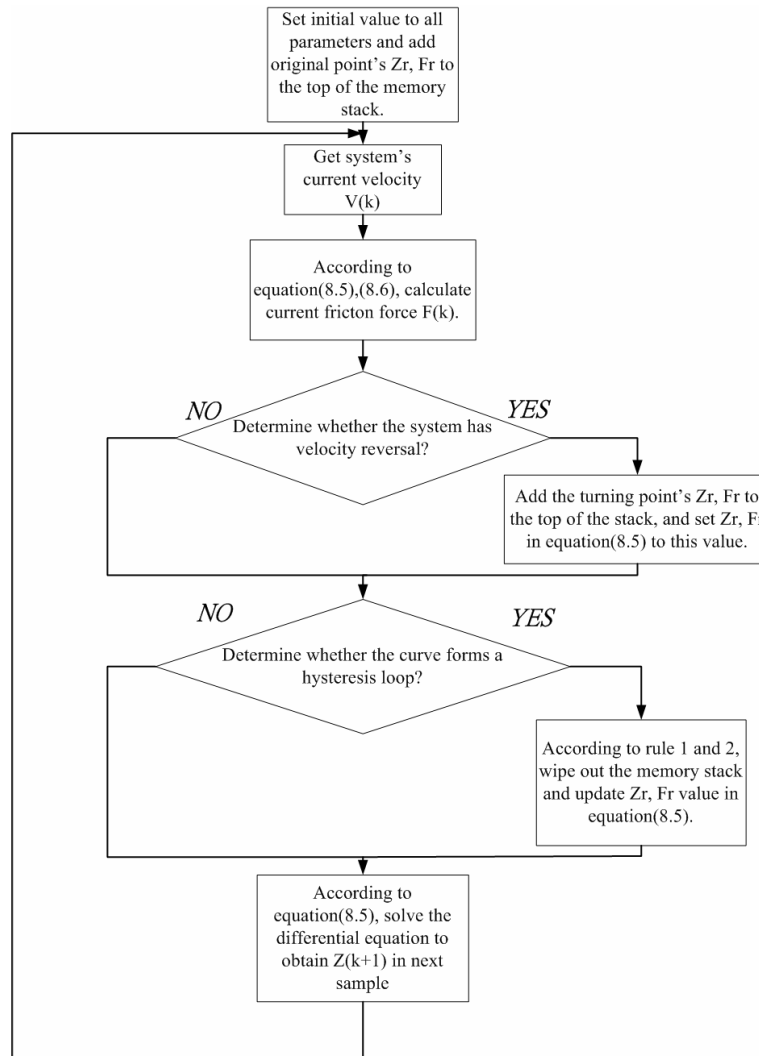


Figure 5.16 The procedure of estimating friction force by the modified friction model.

5.4 Identifying the modified friction model's parameters:

In this section, we will briefly introduce the procedure of identifying parameters k_1 , k_2 , β , and σ_1 .

1. Identification of the nonlinear spring parameters, k_1 , k_2 , β :

If we can estimate or measure solid friction force and bristles' deformation z , we can exploit equation (5.17) to identify these parameters by nonlinear least square method.

[lsqcurvefit(), tool box in Matlab] The goal of the nonlinear least square is to find appropriate value of spring parameters k_1 , k_2 , β that can minimize the error

function $\sum_{i=1}^N [f_i - \hat{f}_i(k_1, k_2, \beta, \hat{z}_i)]^2$. Now the major problem is how to measure the solid friction force and estimate the bristles' deformation z . The solid friction force can be approximately obtained by the following simple experiment. We give a position command in position feedback loop. If the velocity and acceleration response of the system is close to zero, the viscous and inertia term in equation (5.24) can be omitted.

$$J \cdot a = u - f - \sigma_1 \cdot \frac{dz}{dt} - B \cdot v \quad (5.24)$$

So, $f = u$. The control force u is almost equal to solid friction force f . In equation (5.5), the initial value of the solid friction force f_r at an initial point is zero, $f_d(z) = f = u$, and $s(v) = F_s$ in presliding region, then equation (5.5) can be rewritten as below:

$$\frac{dz}{dt} = v \cdot \left(1 - \frac{u}{F_s}\right) \quad (5.25)$$

In the above equation, velocity response v , control force u , and stick force F_s are known, we can solve the differential equation (5.25) to obtain the bristles' deformation z . Therefore, the information about friction force and bristles' deformation z are all known, then we can use nonlinear least square to identify spring's parameters k_1 , k_2 , and β .

2. Identification of the micro viscous parameter σ_1 :

At the beginning of the motion, bristles' deformation is almost equal to system's displacement, we can write down equations (5.26) and (5.27).

$$z = x \quad (5.26)$$

$$\frac{dz}{dt} = \frac{dx}{dt} \quad (5.27)$$

where x is displacement of the system. The initial stiffness of the nonlinear spring

is $k_1 + k_2$. Therefore, we can write down validly the dynamic equation of the system in extremely small range after the beginning of the motion as below.

$$J \cdot \ddot{x} + (\sigma_1 + B) \cdot \dot{x} + (k_1 + k_2) \cdot x = u \quad (5.28)$$

Take the Laplace transform of equation (5.29):

$$\begin{aligned} \frac{X(s)}{U(s)} &= \frac{1}{J \cdot s^2 + (\sigma_1 + B) \cdot s + (k_1 + k_2)} \\ &= \frac{1}{(k_1 + k_2)} \cdot \frac{\omega_n^2}{s^2 + 2 \cdot \xi \cdot \omega_n \cdot s + \omega_n^2} \end{aligned} \quad (5.29)$$

where $\xi = \frac{\sigma_1 + B}{2 \cdot \sqrt{(k_1 + k_2) \cdot J}}$ and $\omega_n = \sqrt{\frac{(k_1 + k_2)}{J}}$.

With a K (Nt) step force applying to the open loop system and considering the system as an over-damped second-order system, we can take inverse Laplace transform of equation (5.29) to obtain the analytic solution of position response $x(t)$ in time domain.

$$\begin{aligned} x(t) = \frac{K}{(k_1 + k_2)} \cdot & \left(1 + \frac{1}{2 \cdot \sqrt{\xi^2 - 1} \cdot (\xi + \sqrt{\xi^2 - 1})} \cdot e^{-(\xi + \sqrt{\xi^2 - 1}) \cdot \omega_n \cdot t} \right. \\ & \left. - \frac{1}{2 \cdot \sqrt{\xi^2 - 1} \cdot (\xi - \sqrt{\xi^2 - 1})} \cdot e^{-(\xi - \sqrt{\xi^2 - 1}) \cdot \omega_n \cdot t} \right) \end{aligned} \quad (5.30)$$

In the above equation, k_1 , k_2 , J , and B are known. Therefore, we can choose proper σ_1 value to make the position response from equation (5.30) to match the measured experimental data. Then, we get the value of micro viscous coefficient σ_1 .

Now, we give a 2 hz, 5 (μm) amplitude sinusoidal position command (equation (5.31)) and collect the data before 0.17 (sec), prior to the point where velocity reversal happens. Then, we can estimate bristles' deformation z and solid friction force. Use nonlinear least square method to identify spring parameters, and obtain

$k_1 = 1.2704 \times 10^6 (N/m)$, $k_2 = 6.1444 \times 10^6 (N/m)$ and $\beta = 1.6110 \times 10^7 (1/m)$ (see figure 5.17 and 5.18).

$$Xr(t) = \frac{A}{2} \cdot \left(1 - \cos\left(2 \cdot \pi \frac{t}{T_p}\right) \right) \quad (5.31)$$

$$A = 5(\mu m), \quad T_p = 0.5(\text{sec})$$

All of the parameters in the modified friction model are listed in table 5.1.

Table 5.1 The value of the parameters of the modified friction model we identified in the experiments.

Symbol and name	value	unit
k_1 , nonlinear spring stiffness(1)	1.2704×10^6	N/m
k_2 , nonlinear spring stiffness(2)	6.1444×10^6	N/m
β	1.6110×10^7	1/m
σ_1 , micro damping (modified friction model)	8.5531×10^3	Kg/sec

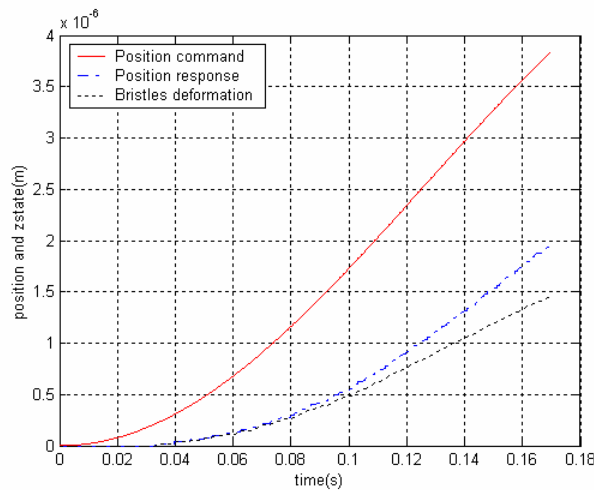


Figure 5.17 Position response and estimated bristles' deformation z .

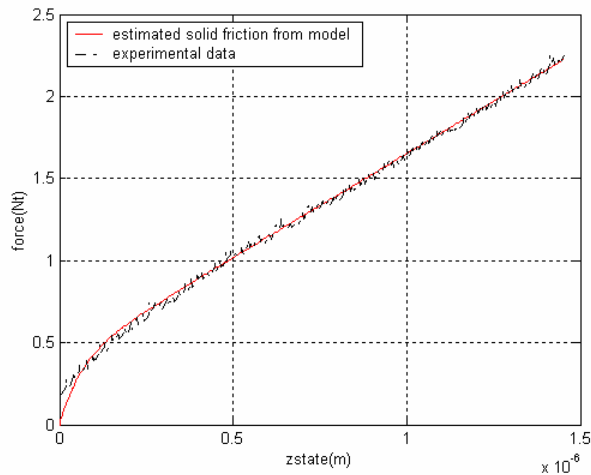


Figure 5.18 Solid friction force vs bristles' deformation z .

Finally, we use a $3(Nt)$ step force command and catch the position response which is less than $0.4(\mu m)$ to identify σ_1 parameter and get $\sigma_1 = 8.5531 \times 10^4 (kg/sec)$ (see figure 5.19).

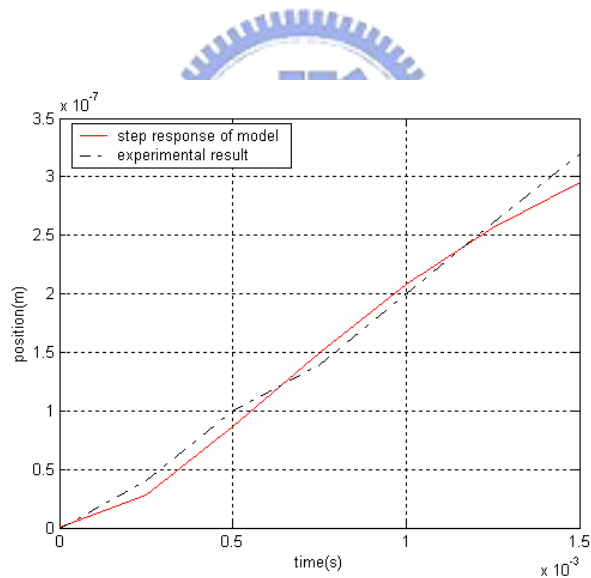


Figure 5.19 A $3(Nt)$ step response for identifying σ_1 .

5.5 Experimental results:

In this section, we will verify the modified friction model's validity by conducting some experiments. The controller structure (see figure 5.20) is divided into three categories:

- (1) traditional controller (tc),
- (2) traditional controller (tc) + feedforward friction compensator based on LueGre model,
- (3).traditional controller (tc) + feedforward friction compensator based on modified friction model.

We will give some position commands to analyze the tracking performance of the three controller structures in both presliding region and sliding region. The performance index we adopt here is listed as below.

$$E_{\max} = \max_{0 \leq t \leq 3.0} |x_r - x| \quad (5.32)$$

$$E_{rms} = \sqrt{\frac{1}{N} \sum_N (x_r - x)^2} \quad , \text{for } 0 \leq t \leq 3.0 \quad (5.33)$$

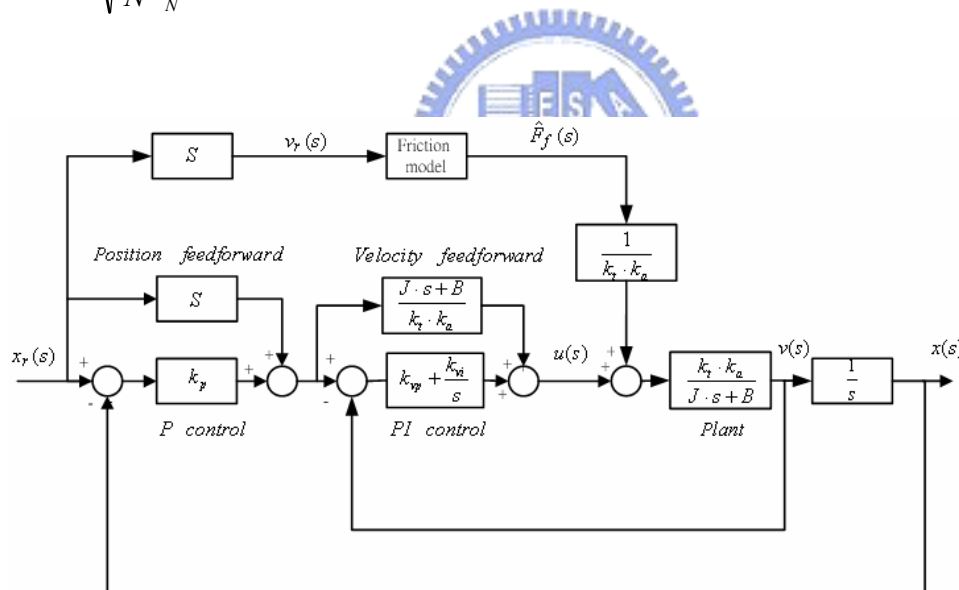


Figure 5.20 Controller structure in experiments

All of the parameters used in the controller are listed in table 5.2, 5.3.

Table 5.2 The parameters of plant and friction

Symbol and name	Value	Unit
J , inertia	2.49	kg
B , viscous friction coefficient	44.14	kg/sec
F_S , static friction force	20.00	N
F_C , Coulomb friction force	4.21	N
v_s , Stribeck velocity	0.005	m/sec
σ_0 , bristle stiffness (LueGre)	1.6484×10^6	N/m
σ_1 , micro damping (LueGre)	1.1861×10^4	kg/sec
k_1 , nonlinear spring stiffness (1)	1.2704×10^6	N/m
k_2 , nonlinear spring stiffness (2)	6.1444×10^6	N/m
β	1.6110×10^7	1/m
σ_1 , micro damping (modified model)	8.5531×10^3	kg/sec
K_t , force constant of motor	28.5	N/A
K_a , gain of current driver	0.349	Volt/A
T , sampling rate	0.00025	sec

Table 5.3 The parameters of the controller

Symbol and name	Value
K_p , position loop P gain	25.1327
K_{vp} , velocity loop P gain	184.0914
K_{vi} , velocity loop I gain	35537

Remark: According to Olsson [93] research, the micro viscous coefficient must decay with velocity to hold dissipative (see equation (5.34), and $v_d = 1 \times 10^{-8} \text{ m/sec}$).

$$\sigma_1' = \sigma_1 \cdot e^{-(v/v_d)^2} \quad (5.34)$$

1) Experiments in presliding region:

1-a) We will give a sinusoidal position command listed in equation (5.31), of

which A is 1 (μm), and T_p is 0.5 (sec). The tracking performance is listed in

table 5.4.

Table 5.4 Performance index of the three controller structure.

Controller structure	Erms (m)	E _{max} (m)
1.TC (tradition controller)	3.6133×10^{-7}	5.7354×10^{-7}
2.TC+FC (LueGre)	1.7872×10^{-7}	3.3878×10^{-7}
3.TC+FC (Modified)	6.8055×10^{-8}	2.2447×10^{-7}

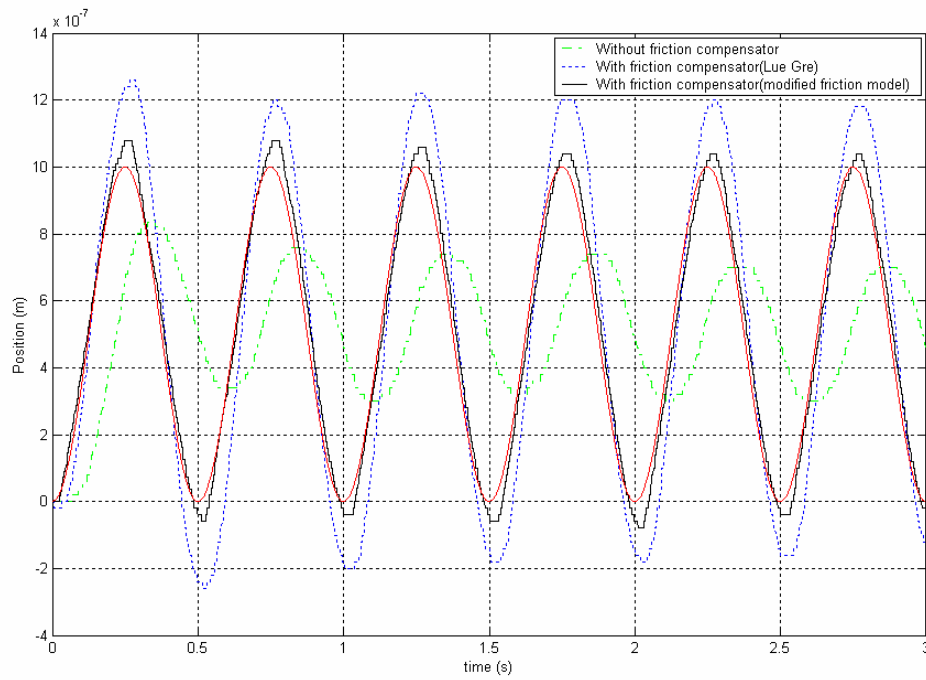


figure 5.21 Position response of the three controller structure.

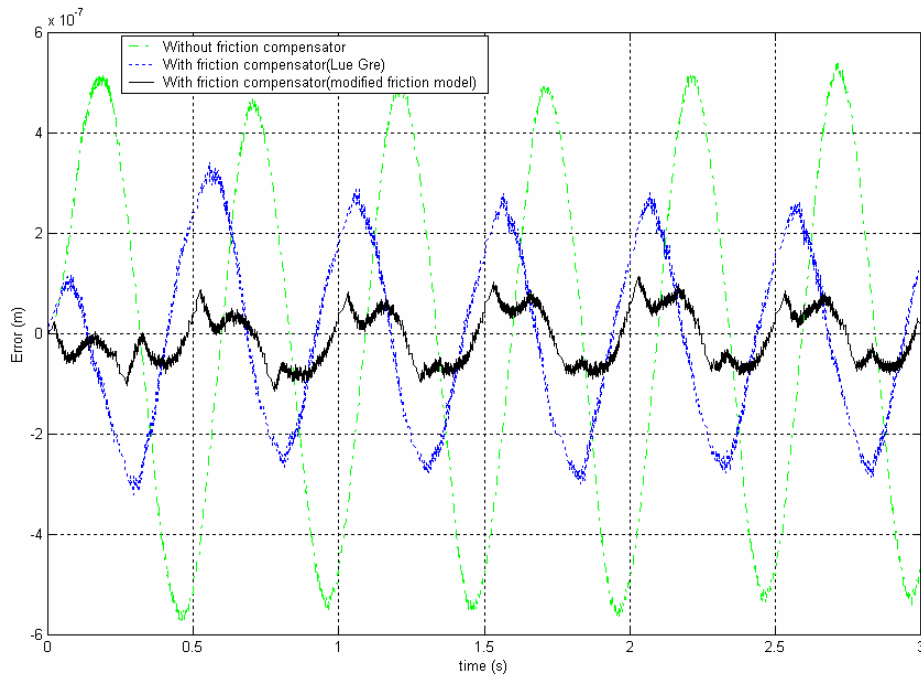


Figure 5.22 Tracking error of the three controller structure.

The friction compensator based on modified friction model decrease the tracking error E_{rms} by 61.92% as compared with the friction compensator based on LueGre model and by 81.17% as compared with the system without the friction compensator. As we expect, the tracking performance of the friction compensator based on modified friction model is much better than the other two.

1-b) We will give a sinusoidal position command listed in equation (5.31), of which A is 5 (μm), and T_p is 0.5 (sec). The tracking performance is listed in table 5.5.

Table 5.5 Performance index of the three controller structure.

Controller structure	Erms (m)	E _{max} (m)
1.TC (tradition controller)	1.4223×10^{-6}	2.3117×10^{-6}
2.TC+FC (LueGre)	7.5682×10^{-7}	1.1968×10^{-6}
3.TC+FC (Modified)	4.1449×10^{-7}	8.0740×10^{-7}

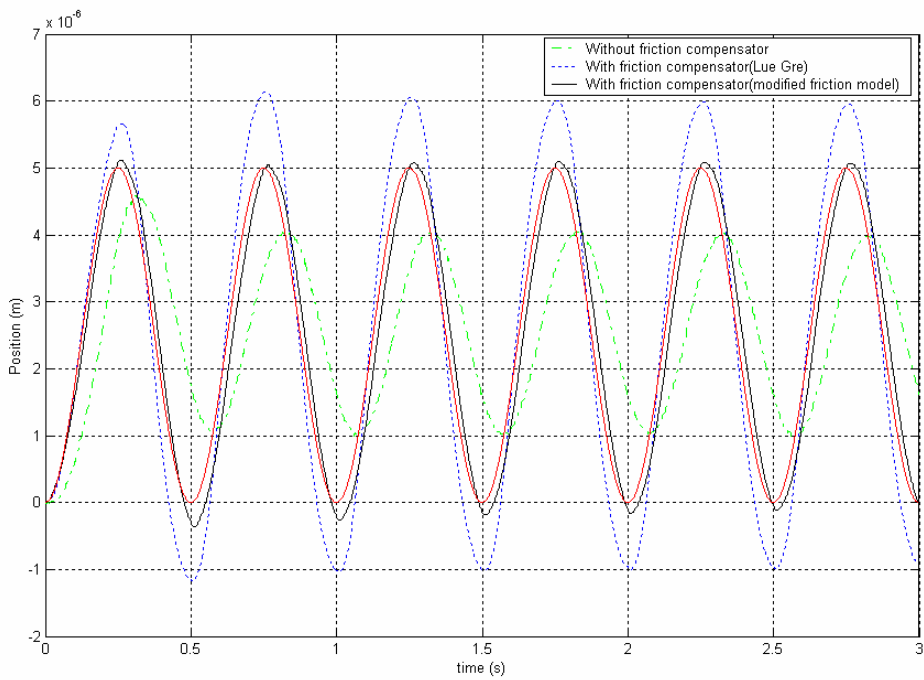


Figure 5.23 Position response of the three controller structure.

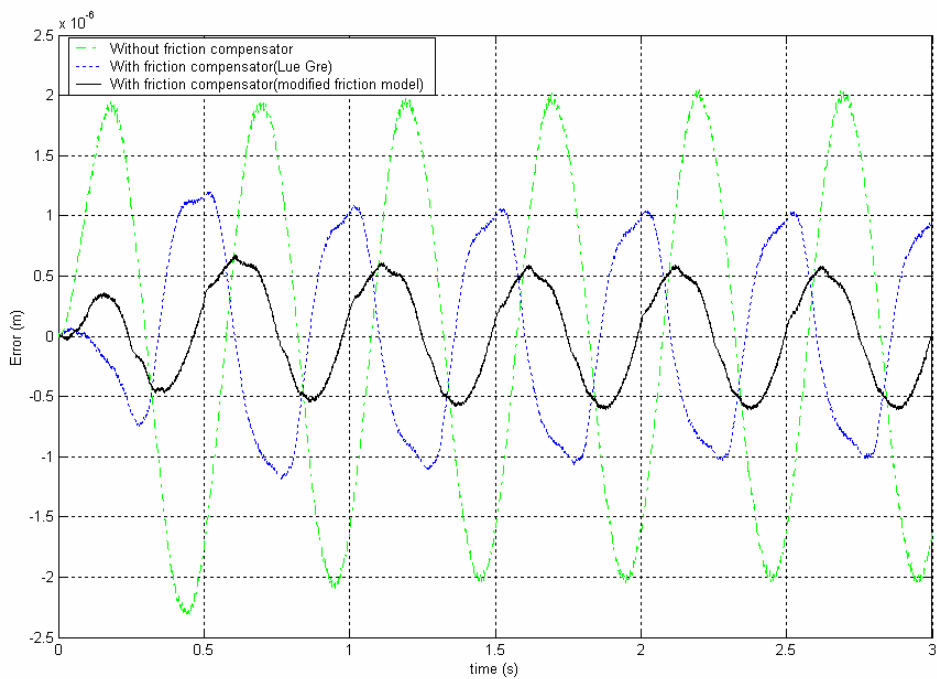


Figure 5.24 Tracking error of the three controller structure.

The friction compensator based on modified friction model decrease the tracking error E_{rms} by 45.23% as compared with the friction compensator based on LueGre model and by 70.86% as compared with the system without the friction compensator. The result is as same as experiment (1-a). The friction compensator based on modified friction model has the best performance.

1-c) We will give a ramp-up and ramp-down position command and check whether the friction-position curve generated by the modified friction model is valid. The tracking performance is listed in table 5.6.

Table 5.6 Performance index of the three controller structure.

Controller structure	Erms (m)	E _{max} (m)
1.TC (tradition controller)	1.5127×10^{-7}	3.040×10^{-7}
2.TC+FC (LueGre)	1.1195×10^{-7}	2.060×10^{-7}
3.TC+FC (Modified)	4.5523×10^{-8}	1.500×10^{-7}

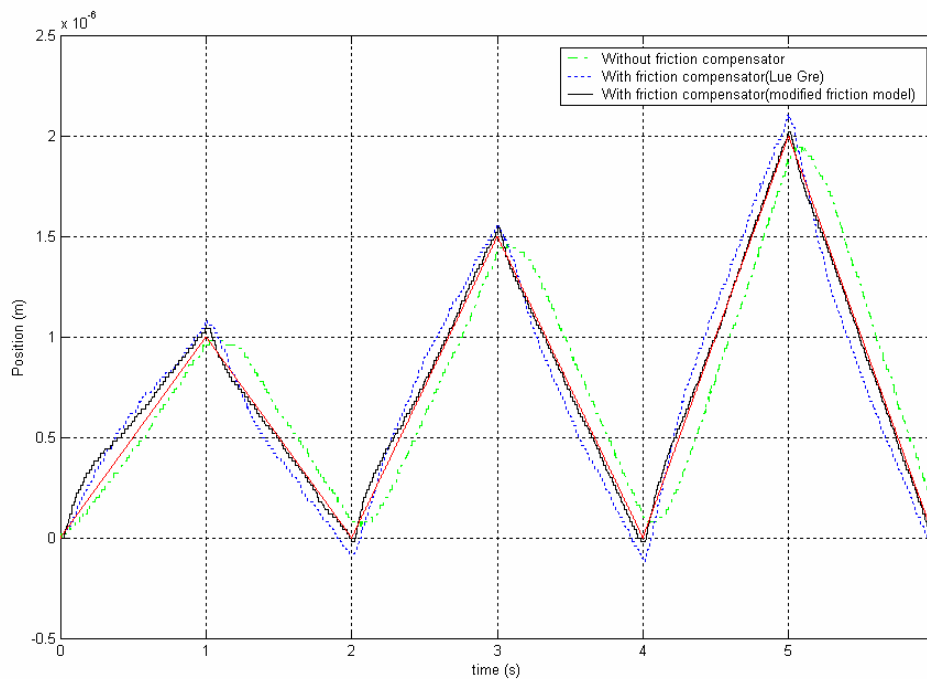


Figure 5.25 Position response of the three controller structure.

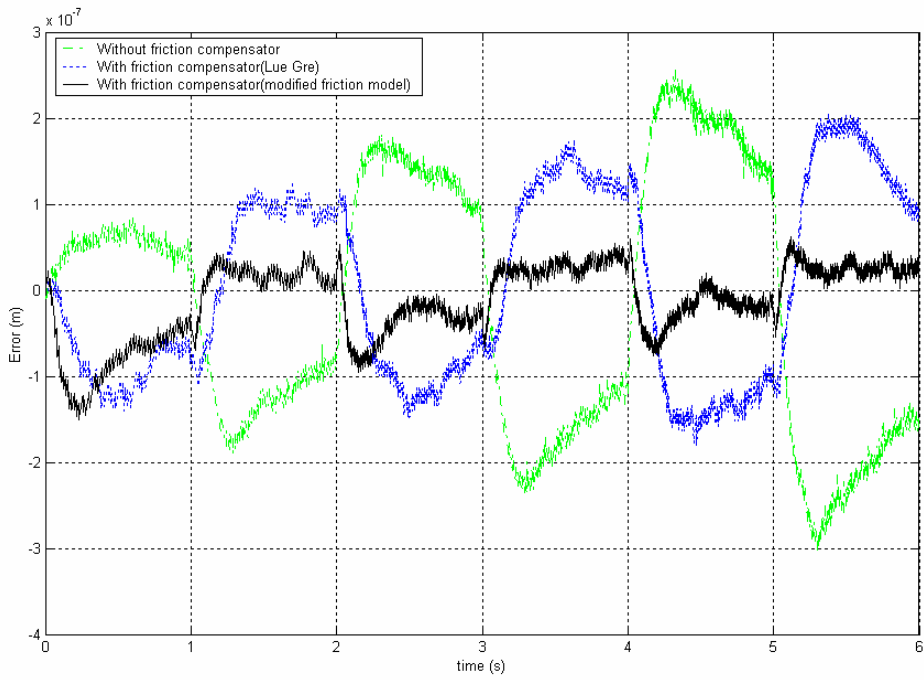


Figure 5.26 Tracking error of the three controller structure.

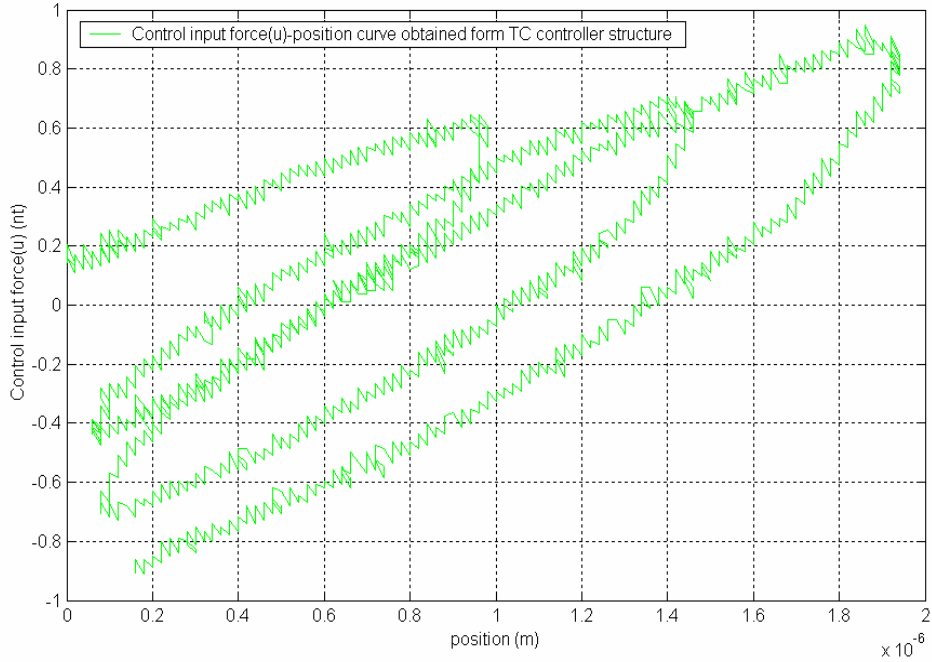


Figure 5.27 Control input force (u) from only TC controller structure versus position

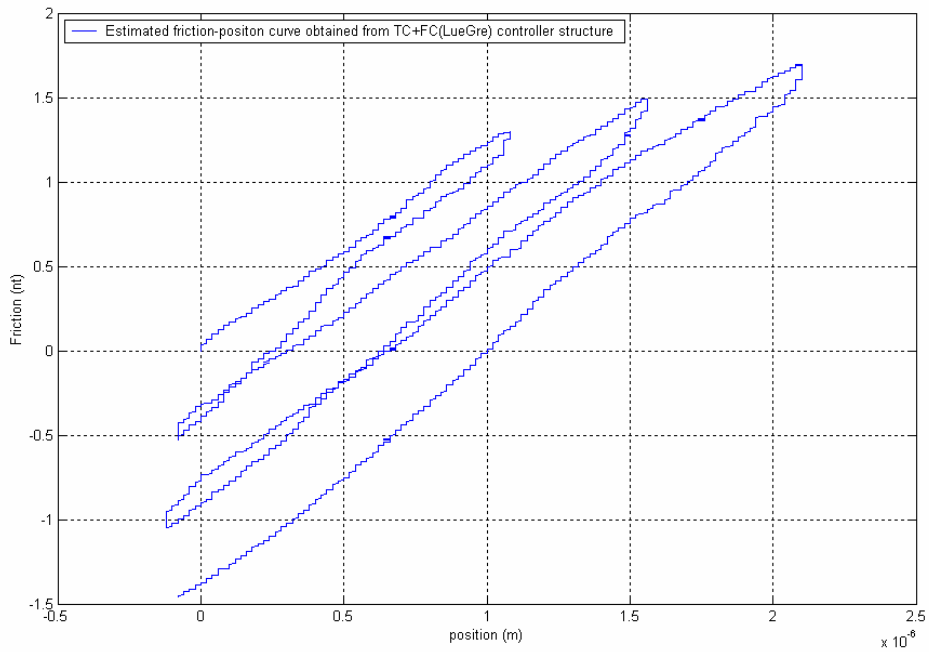


Figure 5.28 Estimated friction force from LueGre model versus position

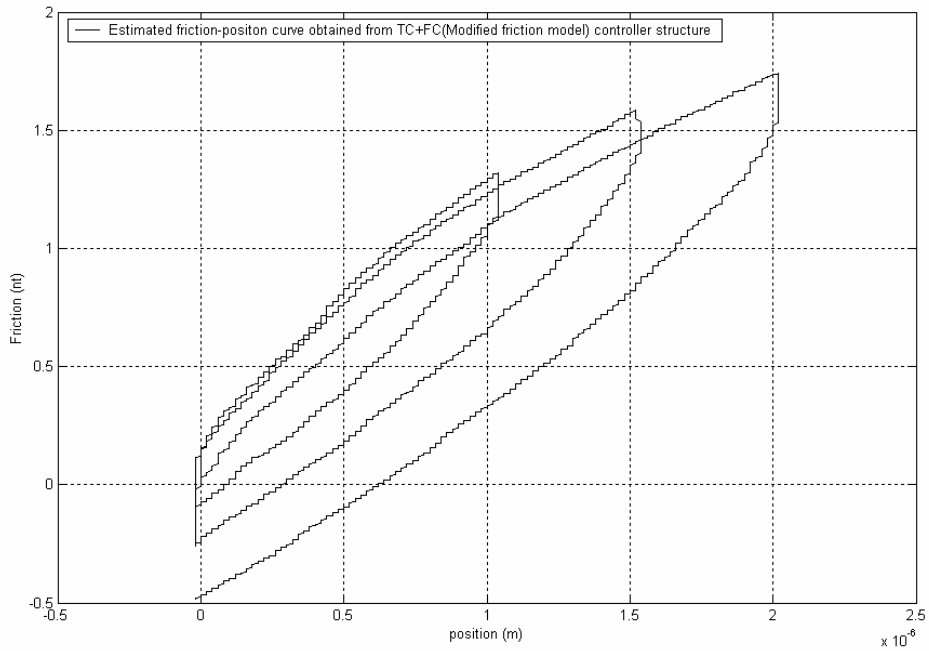


Figure 5.29 Estimated friction force from modified friction model versus position

The friction compensator based on modified friction model decrease the tracking error E_{rms} by 59.34% as compared with the friction compensator based on LueGre model

and by 69.91% as compared with the system without the friction compensator. As we can see from the above experimental results, the friction compensator based on LueGre model can not improve the tracking performance effectively under ramp up and ramp down type position command because the relationship between friction force and displacement predicted by LueGre model is not correct. The control input force in figure 5.27 can be considered as friction force because the velocity and acceleration of the system is extremely small. Because the velocity command (see figure 5.20) fed into the feedforward type friction compensator based on the modified friction model is not the same as the velocity response of the TC controller structure, the friction value estimated by the compensator is different from the real friction force (control input force of TC controller structure), but the estimated friction-position curve is much more similar to the real friction-position curve in figure 5.27 than LueGre model. Obviously, the friction compensator based on modified friction model has the best tracking performance.



2) Experiments in sliding region:

We gave a sinusoidal position command listed in equation (5.31), of which A is 1 (mm), and T_p is 0.5 (sec). This command will make the system slide, so we can analyze the performance of the friction compensator based on modified friction model in sliding region. The tracking performance is listed in table 5.7.

Table 5.7 Performance index of the three controller structure.

Controller structure	Erms (m)	E _{max} (m)
1.TC (tradition controller)	8.8832×10^{-6}	3.1683×10^{-5}
2.TC+FC (LueGre)	4.5728×10^{-6}	1.9841×10^{-5}
3.TC+FC (Modified)	4.5041×10^{-6}	1.9509×10^{-5}

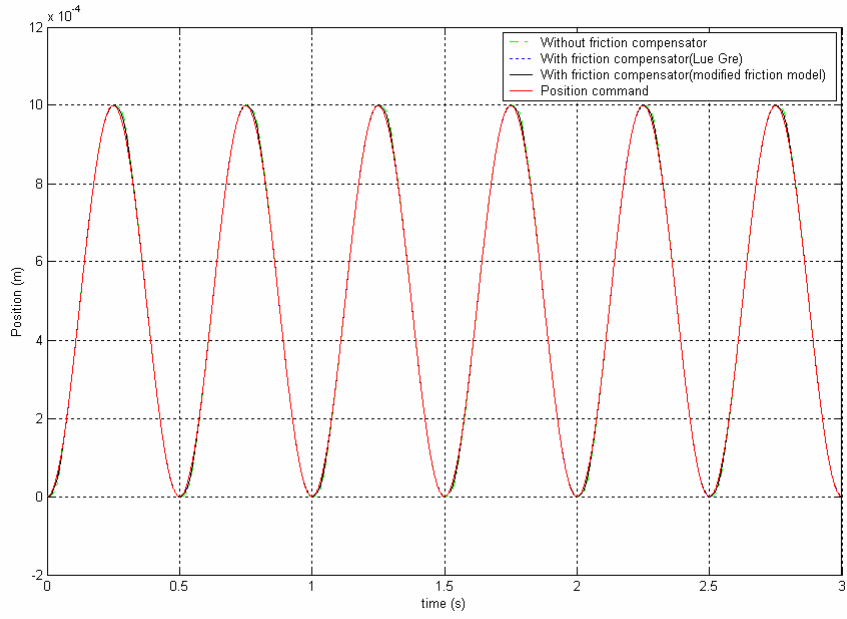


Figure 5.30 Position response of the three controller structure.

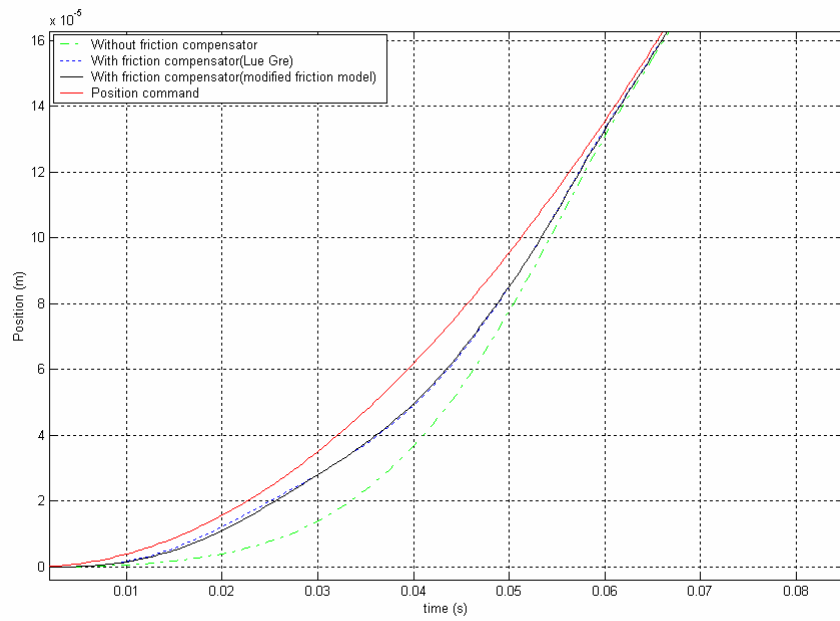


Figure 5.31 Position response at start-up period

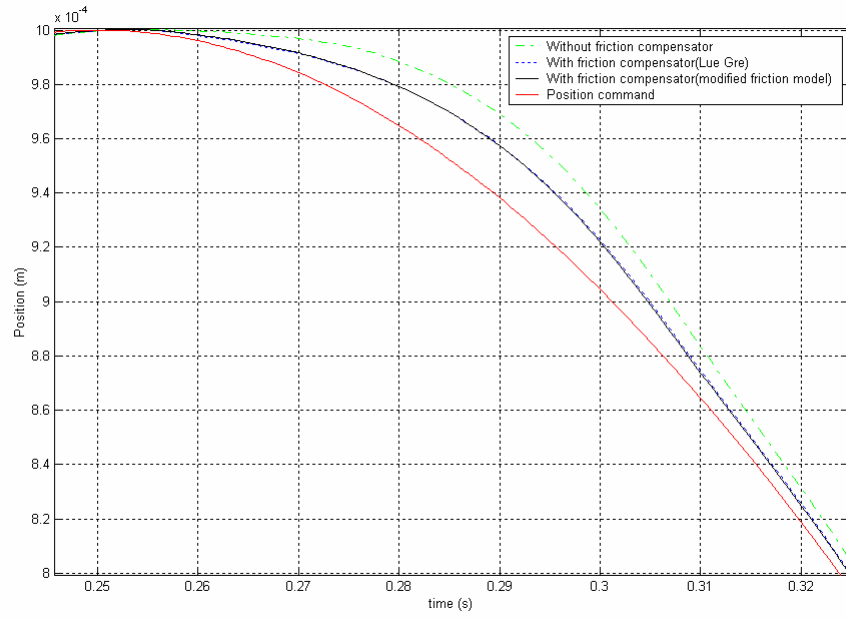


Figure 5.32 Position response near the first velocity reversal

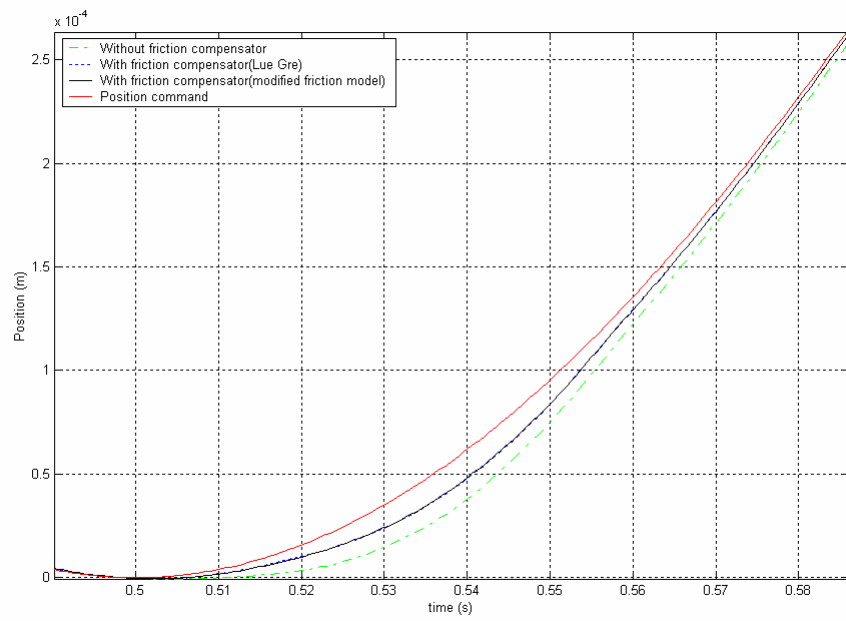


Figure 5.33 Position response near the second velocity reversal

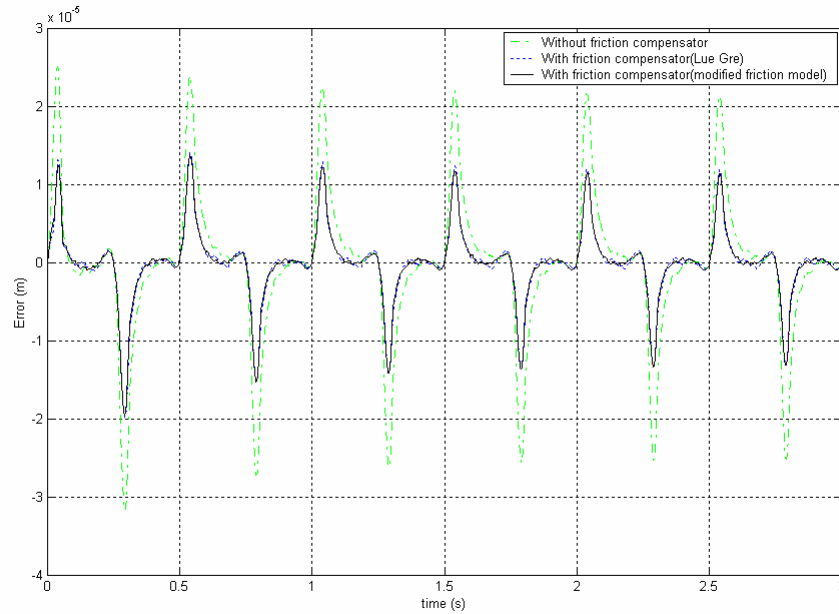
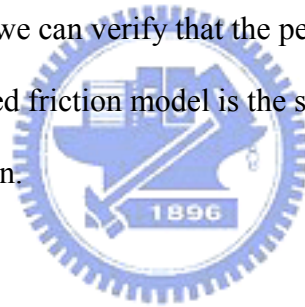


Figure 5.34 Tracking error of the three controller structure.

From the above experiments, we can verify that the performance of the friction compensator based on modified friction model is the same as the one based on LueGre model in sliding region.



5.6 Summery:

In this chapter, we applied a nonlinear spring function to the friction model proposed by Jan Swevers in order to make this model easier to implement and to capture the nonlinear spring phenomenon after velocity reversal more accurately. From experimental results in this chapter, we verify that the modified friction model is superior to LueGre model in presliding region, and they have same performance in sliding region. The future work will be focused on developing a friction observer based on this modified friction model to outperform the performance of the feedforward type compensator based on this model.

Chapter 6

Conclusions and Future Work

6.1 Conclusions

Among the eight control structures compared in Chapter 3, the combination of feed-forward control design plus disturbance observer, and feed-forward-type friction and cogging force compensators is the best. It can significantly improve the control performance as compared with the traditional feedforward design. Nevertheless, disturbance observer generates limit cycles in regulating control, which severely deteriorates its applicability. This thesis derives a sufficient condition for the absence of limit cycles and introduces an adaptive mechanism that can actually solve this problem. Finally, a modified friction model whose performance is much better than the LueGre model in the micro scale region is proposed and several experimental results verify its validity.

6.2 Future work

Most applications of friction models are assumed to be only on two-surface contacting condition. However, there exist several contact surfaces in a controlled mechanical system. For example, a ball-screw-driven system includes many pairs of contact surfaces that induce friction. Between these friction sources, there exist several flexible and inertia elements. To analyze this kind of high-dimension motion system with a single friction model sometimes is not sufficient. However, to identify each friction sources is still a difficult task. Multi-source friction phenomena in a complicated system require further study.

The friction compensator in this thesis is simple feedforward type. Its performance is

influenced by environmental variation and some uncertainties. If we designed the friction compensator which have an adaptive mechanism to cancel the effects of those uncertainties, the system performance and robustness would have to be further improved.



References

- [1] Amin, J., Friedland, B., and Harnoy, A., "Implementation of a friction estimation and compensation technique," *IEEE Control Systems Magazine*, vol. 17, no. 4, pp. 71-76, August 1997.
- [2] Armstrong-Helouvry, B., Dupont, P., and Canudas de Wit, C., "A survey of models, analysis tools and compensation methods for the control of machines with friction," *Automatica*, vol. 30, no. 7, pp. 1083–1138, 1994.
- [3] Armstrong-Helouvry, B., "Control of machines with friction," Kluwer Academic Publishers, Nowell, MA, 1991
- [4] Awabdy, B.A., Shih, W., and Auslander, D. M. "Nanometer positioning of a linear motion stage under static loads," *IEEE/ASME Trans. on Mechatronics*, vol. 3, no. 2, pp. 113-119, 1998.
- [5] Baril, C.G. and Gutman, P.O., "Performance enhancing adaptive friction compensation for uncertain systems," *IEEE Trans. on Control Systems Technology*, vol. 5, no. 5, pp. 466-479, 1997.
- [6] Berger, E.J., "Friction modeling for dynamic system simulation," *ASME J. of Applied Mechanics Reviews*, Vol. 55, no. 6, pp. 535-577, 2002.
- [7] Canudas de Wit, C., Astrom, K.J., and Braun, K., "Adaptive friction compensation in DC-motor drives," *IEEE Trans. on Robotics and Automation*, vol. RA-3, no. 6, pp. 681-685, 1987.
- [8] Canudas de Wit, C., Olsson, H., Astrom, K.J., and Lischinsky, P., "A new model for control of systems with friction," *IEEE Trans. on Automatic Control*, vol. 40, no. 3, pp. 419-425, 1995.
- [9] Canudas de Wit, C., and Lischinsky, P., "Adaptive friction compensation with partially known dynamic friction model," *INT. J. Adaptive control and Signal Processing*, vol. 11, pp. 65-80, 1997.
- [10] Chen, X., Komada, S., and Fukuda, T., "Design of a nonlinear disturbance observer,"

IEEE Trans. on Industrial Electronics, vol. 47, no. 2, pp. 429-437, 2000.

- [11] Cheok, K.C., Hu, H., and Loh, N.K., "Modeling and identification of a class of servomechanism systems with stick-slip friction," *ASME J. of Dynamic Systems, Measurement and Control*, Vol. 110, pp. 324-328, 1988.
- [12] Dahl, P., "Solid friction damping of mechanical vibrations," *AIAA Journal*, vol. 14, no. 12, pp. 1675-1682, 1976.
- [13] de Jager, B., "Acceleration assisted tracking control," *IEEE Trans. on Control Systems Magazine*, vol. 4, no. 5, pp. 20-27, 1994.
- [14] Du, H. and Nair, S.S., "Modeling and compensation of low-velocity friction with bounds," *IEEE Trans. on Control Systems Technology*, vol. 7, no. 1, pp. 110-121, 1999.
- [15] Dupond, P., "Avoiding stick-slip through PD control," *IEEE Trans. on Automatic Control*, vol. 39, no. 5, pp. 1094-1097, 1994.
- [16] Dupont, P., Hayward, V., Armstrong, B., and Altpeter, F., "Single state elastoplastic friction models," *IEEE Trans. on Automatic Control*, vol. 47, no. 5, pp. 787-792, 2002.
- [17] Eborn, J., and Olsson, M., "Modelling and simulation of an industrial control loop with friction," *Proc. of the 4th IEEE Conference on Control Applications*, pp. 312-322, Albany, New York, 1995.
- [18] Friedland, B. and Park, Y.J., *IEEE Trans. on Automatic Control*, vol. 37, no. 10, pp. 1609-1612, 1992.
- [19] Futami, S., Furutani, A., and Yoshida, S., "Nanometer positioning and its micro-dynamics," *Nanotechnology*, v. 1, no. 1, pp. 31-37, 1990.
- [20] Hashimoto, M., Kiyosawa, Y., and Paul, R.P., "A torque sensing technique for robots with harmonic drives," *IEEE Trans. on Robotics and Automation*, pp. 108-116, vol. 9, no. 1, 1993.
- [21] Haessig, D.A. and Friedland, B., "On the modeling and simulation of friction,"

ASME J. of Dynamic Systems, Measurement and Control, Vol. 113, no. 3, pp. 354-362, 1991.

- [22] Hensen, H.A., van de Molengraft, J. G., and Steinbuch, M., "Frequency domain identification of dynamic friction model parameters," *IEEE Trans. on Control Systems Technology*, vol. 10 , no. 2, pp. 191-195, 2002.
- [23] Hensen, H.A., "Controlled mechanical systems with friction", a dissertation of Eindhoven: Technische Universiteit Eindhoven, The Netherlands, 2002.
- [24] Hong, T. and Chang, T.N., "Control of nonlinear piezoelectric stack using adaptive dither," *Proc. of American Control Conference*, pp. 76-80, 1995.
- [25] Hong, K.C., "The design of sliding mode observer for error compensation of a linear motor system," MS thesis in Chinese, Department of Mechanical Engineering, National Chiao Tung University, Hsinchu, Taiwan ,2003.
- [26] Hsieh, C. and Pan, Y.C., "Dynamic behavior and modeling of the pre-sliding static friction," *Wear*, vol. 242, pp. 1-17, 2000.
- [27] Huang, S.J., Yen, J.Y., and Lu, S.S., "Dual mode control of a system with friction," *IEEE Trans. on Control Systems Technology*, vol. 7, no. 3, pp. 306-314, 1999.
- [28] Iannelli, L., Hohansson, K.H., Honsson, U.T., and Vasca, F., "Dither for smoothing relay feedback systems," *IEEE Trans. on Circuits and Systems—I: Fundamental Theory and Applications*, vol. 50, no. 8, pp. 1025-1035, 2003.
- [29] Ishikawa, J. and Tomizuka, M., "Pivot friction compensation using an accelerometer and disturbance observer for hard disk drives," *IEEE/ASME Trans. on Mechatronics*, vol. 3, no. 3, pp. 194-201, 1998.
- [30] Iwasaki, M., Shibata, T., Matsui, N., "Disturbance-observer-based nonlinear friction compensation in table drive system," *IEEE/ASME Trans. on Mechatronics*, vol. 4, no. 1, pp. 3-8, 1999.
- [31] Johnson, C.T. and Lorenz, R.D., "Experimental identification of friction and its compensation in precise, position controlled mechanisms," *IEEE Trans. on Industry Applications*, vol. 28, no. 6, pp. 1392-1398, 1992.

- [32] Karnopp, D., "Computer simulation of stick-slip friction in mechanical dynamic systems", *ASME J. of Dynamic systems, Measurement and Control*, vol. 107, no. 1, pp. 100-103, 1985.
- [33] Kim, J.H., Chae, H.K., Jeon, J.Y., and Lee, S.W. "Identification and control of systems with friction using accelerated evolutionary programming," *IEEE Control Systems Magazine*, pp. 38-47, 1996.
- [34] Kim, N.J., Moon, H.S., and Hyun, D.S. "Inertial identification for the speed observer of the low speed control of induction machines," *IEEE Trans. on Industry Applications*, vol. 32, no. 6, pp. 1371-1379, 1996.
- [35] Kobayashi, S., Awaya, I., Kuromaru, H., and Oshitani, K., "Dynamic model based auto-tuning digital servo driver," *IEEE Trans. on Industrial Electronics.*, vol. 42, no. 5, pp. 462-466, 1995.
- [36] Komada, S., Machii, N. Hori, T., "Control of redundant manipulators considering order of disturbance observer", *IEEE Trans. on Industrial Electronics.*, vol. 47, no. 2, pp. 413-420, 2000.
- [37] Lee, H.S., Tomizuka, M., "Robust motion controller design for high-accuracy positioning systems," *IEEE Trans. on Industrial Electronics.*, vol. 43, no. 1, pp. 48-55, 1996.
- [38] Lee, S. and Asada, H., "Direct adaptive control of force –guided assembly robots using tuned dither," *Proc. of American Control Conference*, pp. 370-374, 1995.
- [39] Lee, S.W. and Kim, J.H., "Robust adaptive stick-slip friction compensation," *IEEE Trans. on Industrial Electronics.*, vol. 42, no. 5, pp. 474-479, 1995.
- [40] Leine, R.I., van Campen, D.H., de Kraker, A., and van den Steen, L., "Stick-slip vibrations induced by alternate friction models," *Nonlinear Dynamics*, vol.16, pp. 41-54, 1998.
- [41] Li, W., and Cheng, X., "Adaptive high-precision control of positioning tables – theory and experiments," *IEEE Trans. on Control Systems Technology*, vol. 2, no. 3, pp. 265-270, 1994.

- [42] Liebst, B.S.; Hulett, W.J, "Extended Kalman filter based friction compensation," *First IEEE Conference on Control Applications*, pp.841-846. 1992.
- [43] Lin, C.L., Shieh, C.C., Tung, P.C., "Robust wavelet neuro control for linear brushless motors," *IEEE Trans. on Aerospace and Electronic Systems*, vol. 38, no. 3, pp. 918-932, 2002.
- [44] Lin, H.I, "The design of friction compensation for a linear motor motion system," MS thesis in Chinese, Department of Mechanical Engineering, National Chiao Tung University, Hsinchu, Taiwan, 2001.
- [45] Lischnsky, P. Canudas de Wit, C., and Morel, G., "Friction compensation for an industrial hydraulic robot," *IEEE Control Systems Magazine*, vol. 19, no. 1, pp. 25-32, 1999.
- [46] Martins, J.A.C., Oden, J.T., and Simoes F.M.F., "A study of static and kinetic friction," *Int. J. Engineering Science*, vol. 28, no. 1, pp. 29-92, 1990.
- [47] Marui, E., and Endo, H., "Friction and wear property improvement by surface modification: effect of electroless plating film and DLC coating," *Industrial Lubrication and Tribology*, vol. 53, no. 5, pp. 186-191, 2001.
- [48] Mita, T, Hirata, M., Murata, K., and Zhang, H., " H_{∞} control versus disturbance-observer-based control," *IEEE trans. on Industrial Electronics*, vol.45, no.3, pp.488-495, 1998.
- [49] Ohnishi, K, "A new servo method in mechatronics," *Trans. Jpn. Soc. Elec. Eng.*, vol. 107-D, pp. 83-86, 1987.
- [50] Otsuka, J. and Masuda, T., "The influence of nonlinear spring behavior of rolling elements on ultraprecision position control systems," *Nanotechnology*, Vol. 9, pp.85-92, 1998.
- [51] Otten, G., de Vries, J.A., van Amerongen, J., "Linear motor motion control using a learning feedforward controller," *IEEE/ASME trans. on Mechatronics*, vol. 2, no. 3, pp. 179-187, 1997.

- [52] Park, E.C., Lim, H., and Choi, C.H., "Position control of X-Y table at velocity reversal using presliding friction characteristics," *IEEE trans. on Control Systems Technology*, vol.11, no.1, pp. 24-31, 2003.
- [53] Panteley, E., Ortega, R., and Gafvert, M., "An adaptive friction compensator for global tracking in robot manipulators," *Systems & Control Letters*, vol. 33, pp. 307-313, 1998.
- [54] Popvic, M.R., Gorinevsky, D.M., and Goldenberg, A.A., "Fuzzy logic controller for accurate positioning of direct-drive mechanism using force pulses," *IEEE Int. Conf. Robotics and Automation*, pp. 1166-1171, 1995.
- [55] Ray, L.R., Ramasubramanian, A., and Townsend, J., "Adaptive friction compensation using extended Kalman-Bucy filter friction estimation," *Control Engineering Practice*, vol. 9, pp. 169-179, 2001.
- [56] Ro, P.I. and Hubbel, P.I., "Model reference adaptive control of dual-mode micro/macro dynamics of ball screws for nanometer motion," *ASME J. of Dynamic Systems, Measurement and Control*, Vol. 115, pp. 103-108, 1993.
- [57] Ro, P.I., Shim, W., Jeong, S., "Robust friction compensation for submicrometer positioning and tracking for a ball-screw-driven slide system," *Precision Engineering*, vol. 24, pp. 160-173, 2000.
- [58] Ryu, J.H., Song, J., and Kwon, D.S., "A nonlinear friction compensation method using adaptive control and its practical application to an in-parallel actuated 6-DOF manipulator," *Control Engineering Practice*, vol. 9, pp. 159-167, 2001.
- [59] Shahruz, S.M., "Performance enhancement of a class of nonlinear systems by disturbance observers", *IEEE/ASME trans. on Mechanics*, vol. 5, no.3, pp. 319-323, 2000.
- [60] Sepehri, N., Sassini, F., Lawrence, P.D., and Ghasempoor, A., "Simulation and experimental studies of gear backlash and stick-slip friction in hydraulic excavator swing motion," *ASME J. of Dynamic Systems, Measurement and Control*, Vol. 118, pp. 463-467, 1996.
- [61] Southward, S.C., Radcliffe, C.J., "Robust nonlinear stick-slip friction compensation,"

- ASME J. of Dynamic Systems, Measurement and Control*, Vol. 113, pp. 639-645, 1991.
- [62] Swevers, J., Al-Bender, F., Ganseman, C.G., and Prajogo, T., "An integrated friction model structure with improved presliding behavior for accurate friction compensation," *IEEE Trans. on Automatic Control*, vol. 45, no. 4, pp. 675-686, 2000.
- [63] Tafazoli, S., de Silva, C.W., Lawrence, P.D., "Tracking control of an electrohydraulic manipulator in the presence of friction," *IEEE Trans. on Control Systems Technology*, vol. 6, no. 3, pp. 401-411, 1998.
- [64] Tan, K.K., Lee, T.H., Huang, S.N., and Jiang, X., "Friction modeling and adaptive compensation using a relay feedback approach," *IEEE Trans. on Industrial Electronics*, vol. 48, no. 1, pp. 169-176, 2001.
- [65] Tarn, Y.S. and Cheng, H.E., "An investigation of stick-slip friction on the contouring accuracy of CNC machine tools," *International Journal of Machine Tools & Manufacture*, vol. 35, no. 4, pp. 565-576, 1995.
- [66] Tataryn, P.D., Sepehri, N., and Strong, D., "Experimental comparison of some compensation techniques for the control of manipulators with stick-slip friction," *Control Engineering Practice*, vol. 4, no. 9, pp. 1209-1219, 1996.
- [67] Teeter, J.T., Chow, M.Y., Brickley Jr., J.J., "A novel fuzzy friction compensation approach to improve the performance of a DC motor control system," *IEEE Trans. on Industrial Electronics*, vol. 43, no. 1, pp. 113-120, 1996.
- [68] Then, E.H., "The study of friction phenomenon for a linear motor stage," MS thesis in Chinese, Department of Mechanical Engineering, National Chiao Tung University, Hsinchu, Taiwan, 2002.
- [69] Tomei, P., "Robust adaptive friction compensation for tracking control of robot manipulators," *IEEE Trans. on Automatic Control*, vol. 45, no. 6, pp. 2164-22169, 2000.
- [70] Tomizuka, M., "On the compensation of friction forces in precision motion control," *Proceedings of IEEE, Asia-Pacific Workshop on Advances in Motion Control*, pp. 69-74, 1993.

- [71] Tung, E.D., Anwar, G., and Tomizuka M., "Low velocity friction compensation and feedforward solution based on repetitive control," *ASME J. of Dynamic Systems, Measurement and Control*, Vol. 115, pp. 279-284, 1993.
- [72] Umeno, T., Hori, Y., "Robust speed control of DC servomotors using modern two degree-of-freedom controller design," *IEEE Trans. on Industrial Electronics.*, vol. 38, no. 5, pp. 363-368, 1991.
- [73] Vischer, D., and Khatib, O., "Design and development of high-performance torque-controlled joints," *IEEE Trans. on Robotics and Automation*, vol. 11, no. 4, pp. 537-544, 1995.
- [74] Walrath, C.D., "Adaptive bearing friction compensation based on recent knowledge of dynamic friction," *Automatica*, vlo. 20, no. 6, pp. 717-727, 1984.
- [75] White, M.T., Tomizuka, M., Smith, C., "Improved track following in magnetic disk drives using a disturbance observer", *IEEE/ASME trans. on Mechanics*, vol. 5, no.1, pp. 3-11, 2000.
- [76] Yan, T., and Lin, R., "Experimental modeling and compensation of pivot nonlinearity in hard disk drives," *IEEE Trans. on Magnetics*, vol. 39, no. 2, pp. 1064-1069, 2003.
- [77] Yang, S., and Tomizuka, M, "Adaptive pulse width control for precise positioning under the influence of stiction and Coulomb friction," *ASME J. of Dynamic Systems, Measurement and Control*, Vol. 110, no. 3, pp. 221-227, 1988.
- [78] Zhu, Z.Q., Xia, Z.P., Howe, D., and Mellor, P.H., "Reduction of cogging force in slotless linear permanent magnet motors," *IEE Proc. Electr. Power Appl.*, Vol. 144, No.4, July 1997.
- [79] Bendat, J. S. and Piersol, A.G., "Engineering Applications of Correlation and Spectral Analysis," John Wiley & Sons, Inc., New York, USA, 1980, p.40.
- [80] Lee, S.H., Song, J.B., "Acceleration Estimator for Low-Velocity and Low-Acceleration Regions Based on Encoder Position Data," *IEEE/ASME Trans. on Mechatronics*, vol. 6, no. 1, pp. 58-64, 2001.

- [81] Choi, H. T., Kim, B. K., Suh, I. H., and Chung, W. K., “Design of robust high-speed motion controller for a plant with actuator saturation,” *ASME J. of Dynamic Systems, Measurement and Control*, Vol. 122, pp. 535-541, 2000.
- [82] Edward, P.C., *Digital filtering*. Houghton Mifflin Co., Chap. 9, 1992.
- [83] Mendel, J. M., *Maximum-likelihood deconvolution: a journey into model-based signal processing*. R.R. Donnelley & Sons, Harrisonburg, Virginia, USA, 1990.
- [84] Johns, T.M. and Soong, W.L., “Pulsating torque minimization techniques for permanent magnet AC motor drives – a review,” *IEEE Trans. on Industrial Electronics*, vol. 43, no. 2, pp. 321-330, 1996.
- [85] Hwang, S.M., Eom, J.B., Hwang, G.B., Jeong, W.B., and Jung, Y.H., “Cogging torque and acoustic noise reduction in permanent magnet motors by teeth pairing,” *IEEE Trans. on Magnetics*, vol. 36, no. 5, pp. 3144-3146, 2000.
- [86] Hwang, S.M., Eom, J.B., Jung, Y.H., Lee, D.W., and Kang, B.S., “ Various design techniques to reduce cogging torque by controlling energy variation in permanent magnet motors,” *IEEE Trans. on Magnetics*, vol. 37, no. 4, pp. 2806-2809, 2001.
- [87] Iwasaki, T., Sato, T., Morita, A., and Maruyama, H., “Auto-tuning of two-degree-of-freedom motor control for high-accuracy trajectory motion,” *Control Engineering Practice*, vol. 4, no. 4, pp. 537-544, 1996.
- [88] “PLATINUM DDL and SERVOSTAR setup Guide,” Document number: M-LN-016-0702, Kollmorgen, a Danaher Motion Company, 06/20/2002,
- [89] “Handbook of AC Servo Systems,” from www.motiononline.com, supported by Automation Intelligence, Inc., Issued: 11/02/2000.
- [90] H. Kobayashi, S. Endo, S. Kobayashi and C.J. Kempf, “Robust Digital Tracking Controller Design for High-Speed Positioning Systems – A New Design Approach and Implementation Techniques,” *IEEE*, 1996.
- [91] T. Claasen, W. F. G. Mecklenbrauker, and J. B. H. Peek, “Frequency Domain Criteria for the Absence of Zero-Input Limit Cycles in Nonlinear Discrete-Time Systems, with Applications to Digital Filters,” *IEEE Trans. on Circuits and Systems*, vol. cas-22, no. 3, march 1975.
- [92] H. Olsson and K. J. Astrom, “Friction Generated Limit Cycles,” *IEEE Trans. on Control Systems Technology*, vol. 9, no. 4, July 2001.

- [93] H. Olsson, and K. J. Astrom, "Observer-Based Friction Compensation," *Proc of the 35th conference on Decision and Control*, kobe, vol. 4, 4345-4350, 1996.
- [94] Shih, Y.T., The High Precision Control for a Linear-Motor-Driven Motion Stage with Friction Compensation, (2004), Doctor Thesis, National Chiao-Tung University, Hsinchu City, Taiwan.
- [95] M. Fischer, and M. Tomizuka, "Application and Comparison of Alternative Position Sensors in High-Accuracy Control of an X-Y Table," *IEEE*,1996.

